Structural Characteristics and Radiative Properties of Tropical Cloud Clusters

L. A. T. MACHADO

Centro Tecnico Aeroespacial, Instituto de Aeronautica e Espaco, São José dos Campos, São Paulo, Brazil

W. B. ROSSOW

NASA Goddard Space Flight Center, Institute for Space Studies, New York, New York

(Manuscript received 30 July 1992, in final form 11 May 1993)

ABSTRACT

By identifying individual tropical cloud clusters in eight months of the International Satellite Cloud Climatology Project data, the size distribution, average cloud properties, and their variation with system size in tropical convective systems (CS) is examined. The geographic distribution of CS shows a concentration over land areas in the summer hemisphere with little seasonal variation except for the major shift of location into the summer hemisphere. When the tropics are considered as a whole or a region is considered over a whole season, CS of all sizes (from individual convective towers at 2–20 km to the largest mesoscale systems at 200–2000 km) form a continuous size distribution where the area covered by the clouds in each size range is approximately the same. Land CS show a small excess of the smallest CS and a small deficit of the largest CS in comparison to ocean CS. Average CS cloud properties suggest two major cloud types: one with lower cloud-top pressures and much higher optical thicknesses, associated with deep convection, and one with higher cloud-top pressures and lower optical thicknesses, associated with the mesoscale stratiform anvil clouds. The anvil cloud properties show some evidence of a further division into optically thicker and thinner parts. The average properties of these clouds vary in a correlated fashion such that a larger horizontal extent of the convective system cloud is accompanied by a lower convective cloud-top pressure, larger anvil cloud size, and larger anvil cloud optical thickness. These structural properties and their diurnal variation also suggest that the smallest CS may represent a mixture of the formative and dissipating stages of CS, while the medium and large sizes are, principally, the mature stage. A radiative transfer model is used to evaluate the local radiative effects of CS with average cloud properties. The results imply that the mesoscale anvil cloud reinforces the diabatic heating of the atmosphere by the convection and may help sustain these systems at night. The radiative effects of the convective clouds, while unimportant to the total effect of the CS at the top of the atmosphere, may reinforce the diurnal variation of convection. Evaluating the radiative feedback of tropical cloudiness on climate is shown to be very difficult because of the significant diurnal and geographic variations of convective system cloud properties.

1. Introduction

Both weather and climate changes depend on how tropical moist convection, with mass motions extending over nearly the whole troposphere, mediates the transfer into the atmosphere of the solar radiation absorbed by the surface. Averaged over the whole tropics, surface heating by solar [shortwave (SW)] radiation is balanced primarily by evaporative cooling (more so over oceans than land), though there are contributions from terrestrial [longwave (LW)] radiative cooling and sensible heat exchanges (more so over land than ocean). The atmosphere is primarily heated by LW radiation from the surface (absorbed by the water vapor) and by latent heating (when precipitation forms), and cools by LW radiation to space. The tropical convective systems that produce most of the precipitation are also responsible for the transport of water vapor into the upper tropical troposphere and for the formation of tropical cloudiness, both of which modulate the radiative heating and cooling rates of both the surface and the atmosphere. Thus, "deep convection" is central in the exchanges of radiative and latent energy in the tropics that determine the state and circulation of the atmosphere.

Individual convective cells (we will refer to these by their classical cloud-type designation, Cb) are about 2–20 km in size and produce a characteristic "cumulonimbus" cloud, "cumulus tower," or "thunderstorm." [See Scorer (1977) for description of cloud formations.] Much of what we know about convection comes from studies of individual examples observed in a series of projects, such as the Thunderstorm Project (Byers and Braham 1949), GARP (Global Atmospheric Research Program) Atlantic Tropical Experiment (GATE, see Leary and Houze 1979; Houze and Betts 1981; Johnson and Houze 1987), Cooperative

Corresponding author address: Dr. William B. Rossow, NASA Goddard Institute for Space Studies, 2880 Broadway, New York, NY 10025.

Convection Precipitation Experiment [CCOPE, see Hobbs (1978) and references in Parsons and Hobbs (1983)], High Plains Experiment (HIPLEX, Leary and Rappaport 1987), and Taiwan Area Mesoscale Experiment (TAMEX, Akaeda et al. 1991). These studies have shown that the smaller-scale (<60 km), shorter-lived (<4 h) weather systems develop when conditional static instability of the atmosphere is produced by radiative heating gradients, surface heat fluxes, and/or large-scale motions. The properties of these smaller systems (updraft strength, vertical extent, rain production, net vertical transports) are all strongly controlled by the larger-scale environment.

Rather than a random spatial arrangement, however, convection often seems to cluster at scales of 20–200 km or to occur in more organized mesoscale (200–2000 km) systems, observed in GATE (Houze 1977, 1982; Frank 1978; Leary and Houze 1979; Gamache and Houze 1982; Johnson 1984), winter Monsoon Experiment (MONEX) (Webster and Stephens 1980; Churchill and Houze 1984), Australian Monsoon Experiment (AMEX, Holland et al. 1986), TAMEX (Jorgensen and LeMone 1989; Johnson and Bresch 1991), and more recently Equatorial Mesoscale Experiment (EMEX, Webster and Houze 1991), for example. At least two styles of organization have been recognized: squall-line or frontal convective systems, characterized by a linear array of convective cells (e.g., Houze 1977; Houze and Betts 1981; Johnson and Houze 1987), and midlatitude mesoscale convective complexes, characterized by a less-organized arrangement of convective cells within the system (Maddox 1980; Velasco and Fritsch 1987; Miller and Fritsch 1991). Some authors have discussed nonsquall types of tropical systems under a variety of other names, such as "convective cloud clusters" (e.g., Leary and Houze 1979; Churchill and Houze 1984; Tollerud and Esbensen 1985; Esbensen et al. 1988). In addition, there are tropical storms that sometimes develop into hurricanes/typhoons, both of which include significant convective components (e.g., Jorgensen et al. 1985).

Although there seem to be many different conditions that favor mesoscale organization (Houze 1989; Cotton and Anthes 1989), a key feature appears to be relatively strong low-level convergence, which precedes the formation of tropical CS by several hours (Frank 1978) and is often associated with wave perturbations at meso- to synoptic scales. However, the larger-scale vertical motions are usually too small to trigger convection, directly (Cotton and Anthes 1989). In the case of squall-line convection, strong frontal character organizes the supply of warm, moist air from ahead of the system into the embedded convective cells that are arranged in parallel lines along the leading edge of the system. Strong vertical wind shear in the environment separates the convective updrafts and downdrafts, so that stronger, larger-scale motions are possible (e.g., Houze 1989; Weisman 1992). Lifetimes of whole systems (6–18 h) exceed that of individual Cb. In the case of midlatitude mesoscale convective complexes, a low-level jet, in an otherwise weak flow regime, supplies warm, moist air from behind the system into the embedded convective motions that reinforce a mesoscale warm-core vortex (Maddox 1983; Cotton et al. 1989). These systems attain sizes of 200–2000 km and sufficient dynamic stability to last 10–20 h, occasionally lasting a couple of days (Velasco and Fritsch 1987). All mesoscale systems have different phase velocities than the initiating disturbance: squall lines propagate faster than the easterly waves over Africa (Payne and McGarry 1977) and midlatitude mesoscale convective complexes move away from the initial large-scale forcing (Maddox 1980, 1983; Cotton et al. 1989).

All of these convective systems have generally been studied as distinct phenomena, though they all involve substantial deep, moist convective motions at scales of 2–20 km that produce the most intense precipitation. The larger systems resemble each other in key ways: more than half of the total rainfall is produced by convection (Houze 1977; Gamache and Houze 1983; Houze 1989) and convection supplies almost three-quarters of the water in an associated, larger area [about 80% of the total, Houze (1982) and Johnson (1984)] stratiform cloud that has its own, weaker circulations (Houze and Hobbs 1982; Gamache and Houze 1983; Miller and Fritsch 1991). Most systems are associated with strong environmental wind shear or significant jets, along with large-scale, horizontal gradients of moisture and temperature that create the conditional instability.

Despite the large number of projects and case studies, we have not yet surveyed the range and systematic variations of the properties of all convective systems occurring in the atmosphere nor the relative populations of each type of system. We also lack a complete understanding of why convection occasionally transforms into mesoscale systems (cf. McAnelly and Cotton 1992). Although satellites provide the viewpoint for such a survey, most satellite studies of tropical convection have used only space–time-averaged radiances or "outgoing longwave radiation" that mix the effects of all high clouds and eliminate any information about cloud structure and evolution. Midlatitude mesoscale convective complexes were first identified in geostationary satellite images (Maddox 1980). Subsequent surveys used the satellite data to identify and track the motions of these systems (Maddox et al. 1981; Maddox 1983; Velasco and Fritsch 1987; Miller and Fritsch 1991). A reduced resolution Meteosat dataset, produced by the International Satellite Cloud Climatology Project (ISCCP), was used to survey squall-line convection over tropical Africa and the tropical Atlantic Ocean (Desbois et al. 1988; Duvel 1990). Fu et al. (1990) showed that satellite radiance measurements could be used to identify more than one type of tropical cloudiness. In particular, the optically thicker clouds

produced by convection can be separated from the optically thinner stratiform and cirrus clouds. This approach has been used to collect statistics on cloud types defined by their top pressure and optical thickness in the ongoing International Satellite Cloud Climatology Project (Rossow and Schiffer 1991).

This study is motivated by recent results from examining the size distribution of all tropical high cloud systems, together, over Africa and the Atlantic, which show that it is proportional to R^{-2}, where R is the radius of a circle with the same area as the high-level clouds (Machado et al. 1992). Moreover, the average cloud-top height of these systems increases systematically with the size of the system. The distribution shape appears stable if statistics are collected over sufficiently large regions and time periods but differs somewhat between land and ocean. There is also noticeable diurnal variation in the size spectrum: over land diurnal variations occur at all sizes, while over ocean variations are important only at the larger sizes.

The purposes of this study are to

1) extend earlier studies of the CS size distribution to the whole tropics and other seasons,
2) search for other systematic variations of the physical properties of CS with size,
3) describe the structures of CS, and
4) estimate the radiative effects of the variations of CS cloud properties.

In this paper we will refer to all tropical high cloud systems as CS [see chapter 10 in Cotton and Anthes (1989) for an excellent review] to indicate that we are including the smaller individual deep convective plumes as well as larger mesoscale convective systems (MCS, e.g., Houze 1989). In section 2 we describe the data used and the method of analysis. In section 3 we present the results of a survey of CS over the whole tropics (±30° latitude), with the exception of the Indian Ocean sector, for January–February and July–August in 1987 and 1988. In section 4 we estimate the radiative effects of the CS variations discussed in section 3. In section 5 we propose a way to understand these results in terms of the life cycle of mesoscale systems. Section 6 presents a summary.

2. Data and analysis method

a. Data from ISCCP

Two previous studies of CS over tropical Africa and the Atlantic Ocean by Machado et al. (1992, 1993) used visible (VIS $\approx$ 0.7 μm) and infrared (IR $\approx$ 11 μm) radiance data from the Meteosat series of weather satellites produced by ESA (European Space Agency) for ISCCP (Schiffer and Rossow 1983). These data are versions of the full resolution imaging dataset sampled to a spatial interval of about 30 km and a time interval of 3 h, similar to the ISCCP stage B3 dataset (Schiffer and Rossow 1985). These studies emphasized midnight images under summer conditions (June, July, August 1983–88) in the latitude range from 5°S to 20°N in the Atlantic–Africa sector, though some studies of the diurnal cycle were performed. Since variations of radiances were not related to changes in the physical properties of the clouds, the interpretation of the results was confined to discussion of the size and the variation with size of the system-average cloud-top temperature (height).

In this study we use the ISCCP stage B3 data from Meteosat, GOES, and GMS (VIS $\approx$ 0.6 μm for GOES and GMS) to identify the cloud clusters in the whole tropical zone and another dataset, called "stage CX data," to analyze the properties of the clouds. The CX data are the pixel-by-pixel results of the ISCCP analysis, including retrieval of cloud physical properties from the radiances. These data are composed of the original radiances from the stage B3 data (Schiffer and Rossow 1985), the results of the cloud detection algorithm (Rossow and Garder 1994a), and the analysis of the radiances by comparison to a radiative transfer model (Rossow et al. 1991). The stage CX data have the same space–time characteristics as the stage B3 data; namely, they represent areas 4–8 km square that have been sampled at 30-km and 3-h intervals. The final ISCCP data products, stages C1 and C2 (Rossow and Schiffer 1991), represent the statistics of the stage CX data reduced to a spatial resolution of about 280 km (stage C1) and to monthly averages (stage C2). Use of physical quantities retrieved from the radiances eliminates variations associated with solar and viewing zenith angle changes with time of day and season and allows for interpretations in terms of changing cloud processes.

Validation studies of the ISCCP analysis are ongoing, particularly those based on regional experiments such as the First ISCCP Regional Experiment (FIRE, Cox et al. 1987) and the International Cirrus Experiment/European Cloud Radiation Experiment (ICE/EUCREX). Comparison of ISCCP cloud detections with surface observations indicates good agreement for all cloud types; verification of the clear-sky radiances inferred in the ISCCP analysis shows that the accuracy of the cloud detections is within 10%, random, with only a small bias over higher-latitude land areas (Rossow and Garder 1994b). The high clouds we are concerned with are generally large scale, optically thick (except for the thinner cirrus), and much colder than the surface, so that their detection is not as difficult as for boundary-layer clouds. Based on radiative model sensitivity studies, Rossow et al. (1989) estimated the uncertainty of retrieved optical thicknesses to be about ±15%; however, differences between ice-crystal and water-droplet phase functions produce larger biases of 25%–50% in optical thickness for low values (<4) in ice clouds (Minnis et al. 1993). The uncertainty in high cloud-top temperatures for optically thicker clouds is about 2 K, associated primarily with the radiance

measurements, but for thinner cirrus (optical thickness less than or equal to 2), the optical thickness bias of the ISCCP analysis will bias the inferred cloud-top temperature warmer by about 10 K (Minnis et al. 1993). Therefore, our temperature threshold to identify high clouds may exclude some very thin cirrus.

Results from the geostationary satellites are used to cover nearly the whole tropics. (Insat data are not available for the Indian Ocean sector from 40° to 100°E.) Data for January–February and July–August 1987 and 1988 are analyzed to examine the seasonal extremes and the effects of El Niño and La Niña on the CS. [See Trenberth and Branstator (1992) for discussion of the transition from El Niño conditions in 86/87 to La Niña conditions in 1988.] Most of our discussion emphasizes noontime results, where both visible and infrared measurements are available; however, CS variations with time of day are also examined.

b. *Analysis method*

The analysis procedure is similar to that described by Machado et al. (1992), with some minor changes, so it is described briefly here. The analysis has five basic steps: 1) identification of image pixels containing high-level clouds, 2) determination of spatial clusters of such pixels, each of which is identified as CS, 3) subdivision of CS into two or three component types of clouds, 4) determination of CS areas and the areas covered by each component cloud type, and 5) collection of cloud property statistics for the whole CS and each component.

1) IDENTIFICATION OF IMAGE PIXELS CONTAINING HIGH-LEVEL CLOUDS

Image pixels containing high-level clouds are identified by brightness temperatures, TIR $\leq$ 245 K, day or night. In Machado et al. (1992, 1993), a range of thresholds from 253 to 207 K was explored, corresponding (approximately) to cloud-top heights (pressures) from about 8 km (550 mb) to 14.5 km (150 mb), respectively. Fu et al. (1990) examined the whole distribution of observed radiances and found a break in the TIR distribution between 240 and 255 K and identified the convective part by values less than or equal to 215 K. The TIR distribution of clouds with visible reflectivities greater than 0.70 is concentrated below TIR = 240 K; clouds included in the temperature range between 240 and 267 K often have reflectances less than 0.6. Both Fu et al. (1990) and Machado et al. (1992) show that their results are not sensitive to the precise TIR threshold value used. Many other studies have used brightness temperature criteria between 240 and 255 K (the latter is equivalent to the use of a threshold of 240 W m^{-2} in outgoing longwave flux datasets) to identify "precipitating" clouds (see Arkin and Ardanuy 1989) or convective clouds (see references in Fu et al. 1990). Maddox (1980) identified mesoscale convective complexes (MCCs) as clouds with TIR < 241 K and the convectively active parts by TIR < 221 K. Miller and Fritsch (1991) review various other choices of these two thresholds used in studies of MCC: all values are within approximately 5 K.

We select a threshold of 245 K (equivalent to a cloud-top height about 9 km or cloud-top pressure about 450 mb) because buoyant parcels of air reaching this level in the tropics must originate from below the 700-mb level. Such clouds are, therefore, produced directly by convective motions or by the associated mesoscale motions in the middle troposphere that occur in larger CS. By using TIR instead of the retrieved cloud-top temperatures, which are corrected for the effects of emissivities less than 1 in the daytime ISCCP analysis, we lose some of the thinner cirrus clouds. However, the difference in CS area inferred with corrected and uncorrected cloud-top temperatures during the daytime is less than 5%.

2) DETERMINATION OF PIXEL CLUSTERS

Clusters of pixels containing high-level clouds are identified by testing for adjacent pixels that have passed the threshold and for regions devoid of high-level clouds surrounding candidate clusters on all sides by using a technique similar to that used by Wielicki and Welch (1986). All of these clusters are identified as CS, including individual isolated pixels. The study by Machado et al. (1992) shows that clusters of similar size are separated by distances that are typically 4–12 times their radius (where the lower ratio applies at higher temperature thresholds), whereas for a threshold of 207 K, the separation distance is 15–20 times the radius.

3) SUBDIVISION OF CS INTO COMPONENT CLOUD TYPES

Once the cloud clusters are identified, their physical properties are obtained from the ISCCP CX dataset. As we show in section 3a, the shapes of the distributions of cloud properties (ALB—cloud spherical albedo and TC—cloud-top temperature) in the larger CS suggest at least two different components (cf. Fu et al. 1990). The portion of the CS with ALB > 0.70 (optical thickness—TAU > 23) is identified as the deep convective cloud, representing the equivalent of Cb embedded in the CS. The remainder of the CS is identified as the "mesoscale anvil cloud" (MAC). The MAC is further divided into a thicker part, 0.50 < ALB $\leq$ 0.70 (9 < TAU $\leq$ 23), and a thinner part, ALB $\leq$ 0.50 (TAU $\leq$ 9). We refer to the thinner portion as the cirrus anvil cloud (CAC) and the thicker portion as the "transition" anvil cloud (TAC). Diurnal variations of the Cb and the MAC components of the CS can be monitored sep-

arately because the active convective cells produce a characteristic dome with colder cloud-top temperatures than the mesoscale clouds (Cotton and Anthes 1989). Using daytime data (section 3a), we can define characteristic temperature ranges for the two parts of the CS (following Fu et al. 1990): we use TC $\leq$ 215 K to identify Cb and 245 K $\geq$ TC $>$ 215 K for MAC. In the diurnal analysis the mesoscale cloud is not subdivided.

4) Area and size determination

Areas of whole CS and the embedded Cb are determined by separate analyses that count the number of image pixels composing each object and assign an area of 30 km $\times$ 30 km to each pixel. The actual satellite image pixel areas are 5 km $\times$ 5 km; however, uncertainties in navigation limit location accuracy to about 15–30 km, so individual pixels are mapped into a grid with a cell size of about 25–30 km in the ISCCP CX dataset. In effect, we assume that a single pixel within this area represents the whole area statistically. This interpretation is valid for larger ($>$100 km) objects. For smaller CS, composed of only a few pixels, this assumption probably overestimates the size by an amount inversely proportional to the number of pixels in it. The smaller actual size of the image pixels means that we can properly identify the presence of such small CS but not measure their sizes very well. This problem does not affect the size distributions, however, since the smallest size category is interpreted to include all CS sizes from 0 to 60 km.

The sizes of CS and Cb are represented by the radius of an equivalent area circle, $R = (A/\pi)^{1/2}$. The effect of increasing (decreasing) temperature thresholds is to increase (decrease) the values of R. Based on results from Fu et al. (1990) and Machado et al. (1992), the effect of varying the threshold from 230 to 267 K is to increase the CS area by about 20%–30%, which would change the CS radius by 10%–15%. However, the size distributions do not change shape significantly (Machado et al. 1992), so we attach more significance to relative comparisons of size than to the quantitative accuracy of the sizes themselves. In any case, we find that the natural variation of sizes within any particular size category of CS is larger than these uncertainties. The CS size classes are defined by 60-km radius intervals and the Cb size classes by 30-km intervals.

5) Cloud-property statistics

The ISCCP CX data contain values of cloud optical thickness (TAU), cloud-top temperature (TC), and cloud-top pressure (PC) for each image pixel. Values of TAU can also be converted to visible spherical albedos (ALB), which are nearly the total albedos of the cloud, and water path (WP, water content per unit area). Also, the visible radiances (VIS) and cosine of the solar zenith angle (MU0) are available to calculate cloud visible reflectances (Refl = VIS/MU0). These quantities are averaged over whole CS as well as for the component parts.

c. *Radiative flux calculations*

To assess the radiative effects of the CS and their component parts, we calculate surface and top of atmosphere, upwelling and downwelling, shortwave (SW) and longwave (LW) fluxes using the radiation code of the Goddard Institute for Space Studies climate GCM (Hansen et al. 1983; Lacis and Oinas 1991), which has been and is being tested as part of the International Comparison of Radiation Codes in Climate Models (ICRCCM) project (Ellingson and Fouquart 1991; Fouquart et al. 1991; Fels et al. 1991). The atmospheric properties are specified by the tropical standard atmosphere (*U.S. Standard Atmosphere, 1976*) and the surface properties are inferred from the ISCCP analyses. The average cloud properties are obtained in this study.

Two additional assumptions are required for these calculations: the location of cloud bases and the vertical distribution of cloud water within cloud layers. The convective part of the CS is assumed to have a base at 900 mb near the top of the tropical boundary layer, while the mesoscale anvil cloud is assumed to have a base at 600 mb [e.g., Gamache and Houze (1982, 1983) use 900 mb and 650 mb]. The cloud water is distributed proportionally to pressure within each cloud layer.

We assess the radiative effects of the CS in two ways. First, we calculate the actual local perturbations of radiative heating–cooling rates, which might affect the dynamics of the individual systems. Second, we scale the local effects by the total areal coverage of such systems in the tropics and by an approximate lifetime of 1 day to estimate their effect on the large-scale circulation and climate. To average the radiative effects during one day we take into account the ocean albedo variation with the solar zenith angle (Hansen et al. 1983) and a monthly mean diurnal variation of the surface temperatures from ISCCP results. We also investigate the effects of diurnal variations of the CS cloud properties and of systematic variations of CS cloud properties with system size on inferences of the daily mean radiative fluxes.

3. Results

a. *Geographic distribution of CS*

Figure 1 shows the number of tropical CS per day identified by our analysis in 5° $\times$ 5° map cells for 1987–88 in July–August and January–February (hereafter, Jul–Aug and Jan–Feb). Well-known concentrations of convective activity are apparent with peak frequencies greater than 10 per day occurring over land areas. The

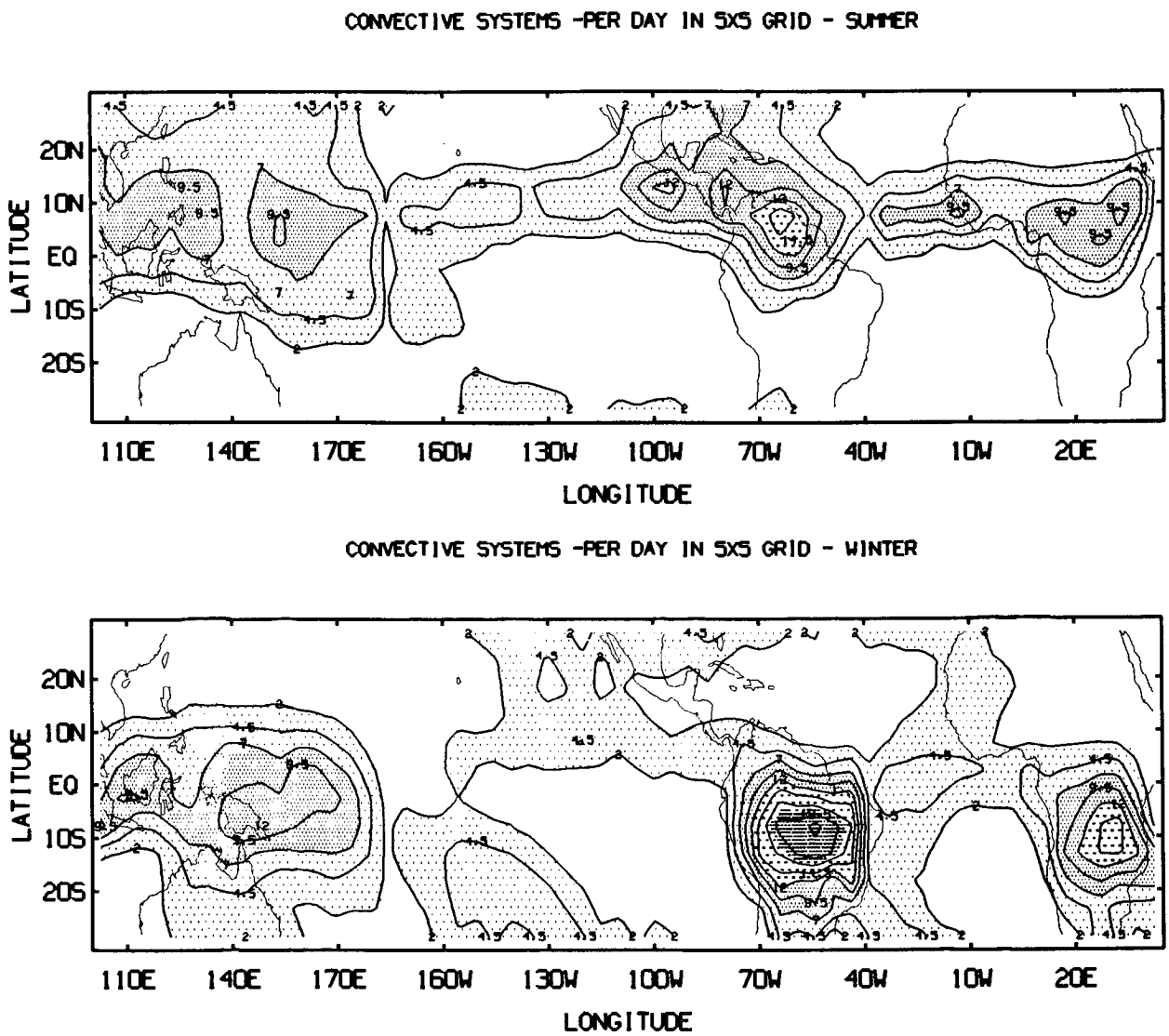

FIG. 1. Maps of the average number per day of convective systems occurring in 5° × 5° latitude–longitude regions in the tropics for (a) summer (July–August 1987 and 1988) and (b) winter (January–February 1987 and 1988). Lowest contour is 2 per day.

largest of the three major peaks is over South America and the smallest is over Indonesia. Both land peaks are larger, and the western Pacific peak covers a larger area in Jan–Feb. Most, but not all, of the convective activity is located north (south) of the equator in Jul–Aug (Jan–Feb).

The distribution of tropical cumulonimbus clouds is described in a global, long-term cloud climatology based on surface weather observers' identifications of cloud morphologies (Warren et al. 1986, 1988). The distribution is concentrated into smaller areas over land than over ocean: frequencies of occurrence are greater than 10% almost everywhere over tropical oceans but only in limited areas over land. However, the peak frequencies over ocean rarely exceed 30%, whereas they often exceed 40% over land. If we isolate Cb in our results, the geographic distribution is essentially identical to that shown in Fig. 1 and very similar to the surface observation climatology of cumulonimbus clouds. The Warren et al. distributions differ from the distribution in Fig. 1 in that they show more concentration over the islands in the western Pacific.

Mesoscale convective complexes are more numerous over land than ocean (Velasco and Fritsch 1987; Miller and Fritsch 1991), suggesting that the particular conditions needed to organize convective motions are more prevalent there. Figure 1 shows that all CS are more numerous over land than ocean. The distributions of CS divided into three size ranges (small—$R < 180$ km, medium—$180 < R < 360$ km, and large—$R > 360$ km) show the same patterns as in Fig. 1, with a concentration of the larger CS into narrower latitude zones.

Notable but small differences in the distributions of the three size ranges, compared with the total CS distributions in Fig. 1, are 1) the smallest CS appear to be less frequent over the ocean to the west of Central America than the larger CS, 2) the medium-sized systems are relatively more frequent in the eastern Pacific, 3) the medium and large CS seem to occur farther from the equator than the smaller CS, and 4) the largest CS occur much less frequently in Africa than in either South America or the western Pacific.

b. Tropical CS size distribution

The structural characteristics of tropical cloud clusters over Africa and the Atlantic Ocean were studied by Machado et al. (1992). Analyzing Meteosat data from six summers (June–July–August), they found that the cloud cluster number in a size interval, $N(R)$, can be approximated by a power law with an exponent of -2. This size distribution means a nearly equal area is covered by each radius class up to a "break radius" where the size distribution slope becomes much steeper. The ISCCP B3 and CX datasets are used to extend these results to the whole tropics (except the tropical Indian Ocean region) and to the winter season.

Figure 2 shows for each satellite region the distributions of CS number and population fraction (at local noon) as functions of CS radius, averaged over Jul–Aug and Jan–Feb 1987–88. The CS number distribution has the same slope (about -2) for all regions. The CS number is expressed as the average number of systems per day in 60-km size intervals within a region defined by 30°N and 30°S and the longitude interval for which the satellite zenith angle is less than 69° (about 80° of longitude). The distribution of CS population fraction (or area fraction relative to all CS) for the whole tropics has the same characteristics found in the Meteosat region.

As shown more clearly in Fig. 2b, the smaller CS ($R < 180$ km) and larger CS ($R > 360$ km) deviate somewhat from the area-conserving distribution of the medium-sized CS; thus, the smaller CS cover somewhat more area (about 40% of the total) and the larger CS cover somewhat less area (about 26%) than the medium-sized CS (about 34%). (The fractions in Fig. 2b represent the percentiles of the total cloud fraction for each radius class and, thus, do not give information about the total cloud cover.) Figure 3a shows that these deviations are larger over land than ocean. (This explains why the deviations are smaller for the GOES-West region, which is principally oceanic.) The ocean CS size distribution is much closer to an R^{-2} distribution over the whole size range than the distribution over land. We show in the following that this behavior is related to the diurnal cycle over land: local noontime is characterized by the beginning of a large increase in the number of smaller cells, particularly associated with topography, which develop into larger systems closer to local midnight (Machado et al. 1993).

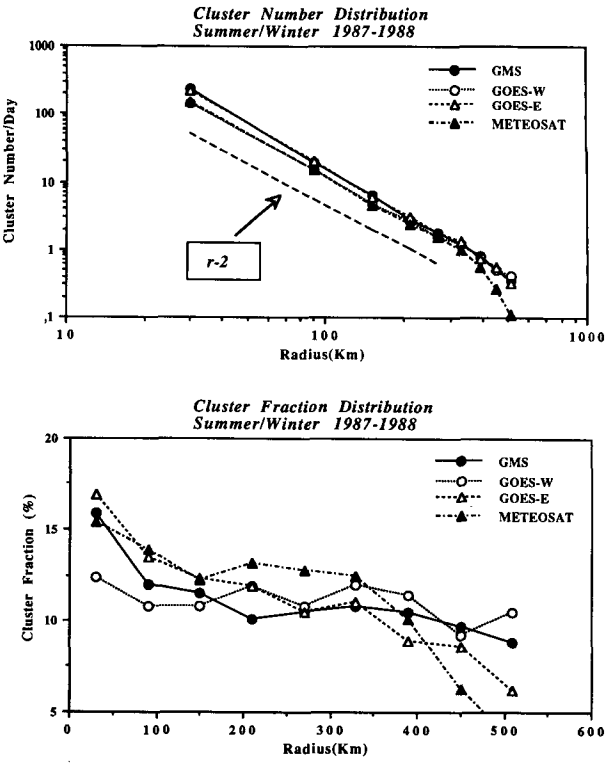

FIG. 2. Average distribution (a) of the number of convective systems with cloud cluster radius and (b) of the ratio of area covered by each size cluster to the total area covered by all convective systems. Results are for images at local noon with January, February, July, and August 1987 and 1988 combined.

We also observe in Fig. 2b a secondary increase in the CS population near the 200-km size, which the previous study of the Meteosat region showed is caused by an enhancement of the mature stage of mesoscale systems in the trough phase of easterly waves (Machado et al. 1993). Although it is difficult to determine the significance of the secondary peaks in the size distributions for the other satellite regions, the similarity to the Meteosat results suggests that CS with radii between 200 and 300 km correspond to developed mesoscale systems over the whole tropics. Miller and Fritsch (1991) identify a preferential size around 300 km (effective radius) for mesoscale convective complexes in the Americas and the tropical western Pacific.

The larger CS appear more frequently in the GMS and GOES-West regions (Fig. 2b). Nakasawa (1988) observed larger systems (around 1000 km in diameter) in the Pacific moving eastward, whereas the embedded smaller-scale systems in these supercloud clusters moved westward with the easterly waves.

Figure 3b shows the CS size distributions for Jul–Aug and Jan–Feb. Since the actual seasonal changes at most locations are dominated by very large latitudinal shifts in the intertropical convergence zone (ITCZ) over land and by somewhat smaller changes

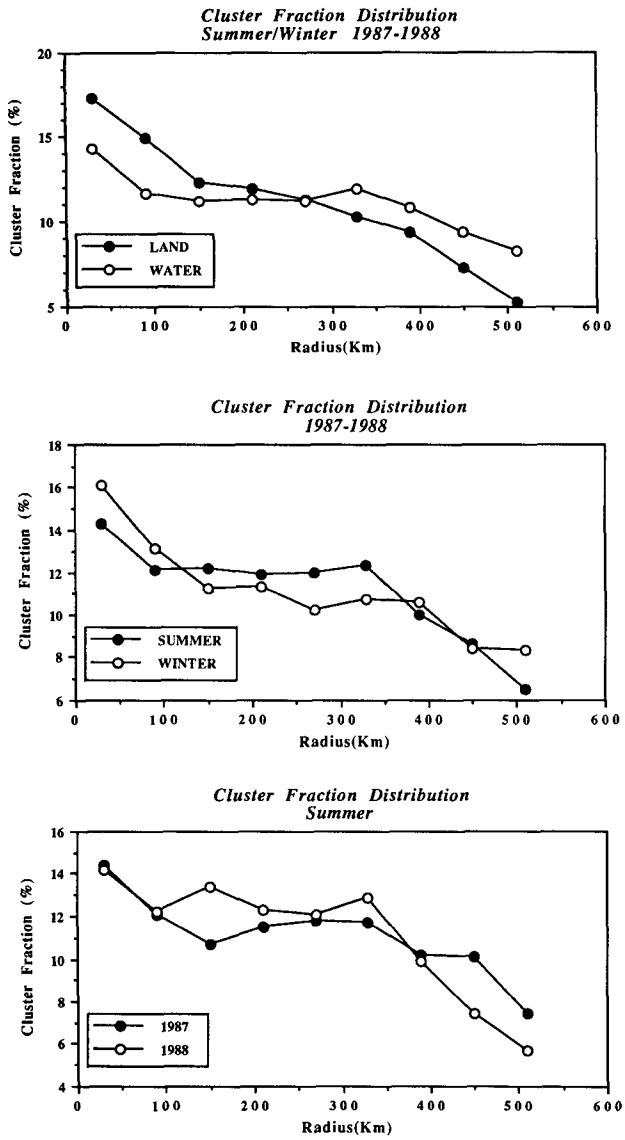

FIG. 3. Distributions of the ratio of area covered by each size cluster to the total area covered by all convective systems (a) for land and ocean averaged over both seasons and years, (b) for January–February and July–August averaged over land and ocean and both years, and (c) for 1987 and 1988 averaged over land and ocean for July–August at noontime.

over ocean (Fig. 1), study of the seasonal variation of convection and, in particular, the mesoscale CS is primarily a study of summer meteorology. Therefore, we consider the aggregate properties of CS over the whole tropics, which are dominated by the summer hemisphere. The differences between Jul–Aug and Jan–Feb are dominated by the changing proportions of land and ocean between the hemispheres rather than a change in CS characteristics with season.

Machado et al. (1992) studied the variation of CS size distributions among the boreal summers of 1983–88 and found several small changes: 1) the probability of finding at least one CS in each size class in the whole region is most variable for the largest sizes; 2) 1984 exhibited more low-level (high TC) CS than in other years; and 3) 1983 exhibited a lower number density of small and medium CS than other years. In this study we compare the distributions in an El Niño and La Niña year, including the region with the most important cloud cover changes (Pacific). Figure 3c shows that the 1987 and 1988 CS size distributions in Jul–Aug are quite similar, despite the large differences in the location of high cloud amount and precipitation (Janowiak and Arkin 1991). In 1988 there is a larger relative fraction of medium-sized CS that is offset by a smaller fraction of large CS. Similar behavior occurs in Jan–Feb of these two years. This suggests that El Niño year conditions may be more favorable to the development of larger CS than La Niña year conditions; however, we note that the magnitude of this difference is not very different from the magnitude of natural interannual variability observed in the Meteosat region (Machado et al. 1992), so that no conclusion about the significance of this difference is possible with this limited dataset.

Figure 3 shows that the difference between land and ocean CS size distributions is larger than that between seasonal or interannual distributions. Thus, we focus on characterizing land–ocean differences.

c. *Variation of CS physical properties*

1) STRUCTURE OF CS

Figure 4 shows the aggregated distributions of TC and ALB from individual image pixels within CS of different sizes. We examined all of the *individual* CS histograms in July 1987 for the larger cluster sizes ($R > 180$ km) and found that the features (e.g., multiple maxima) shown in Fig. 4 are not produced by a mixture of CS cloud properties from different regions and times but represent typical features present in most individual CS. The TC and ALB distributions for the smallest CS category are, however, produced by a mixture of two different types (see the following).

The TC histogram (Fig. 4a) shows a systematic shift in the distribution from warmer temperatures for the smaller CS to colder temperatures for the larger CS. The medium CS all exhibit a broad, monomodal distribution of TC with a mode value near 230 K and a long tail out to 180 K. The TC distribution of the smallest CS indicates a bimodal distribution: the largest population has TC values from 225 to 245 K, but there is a small population with TC < 200 K.

The ALB histogram (Fig. 4b) shows three distinct maxima for all but the smallest sizes of CS and some variation of the relative proportion of each ALB group with CS size. The largest ALB maximum (ALB near 0.84) contains image pixels that are almost all colder than 220 K; thus, we identify these clouds as convective

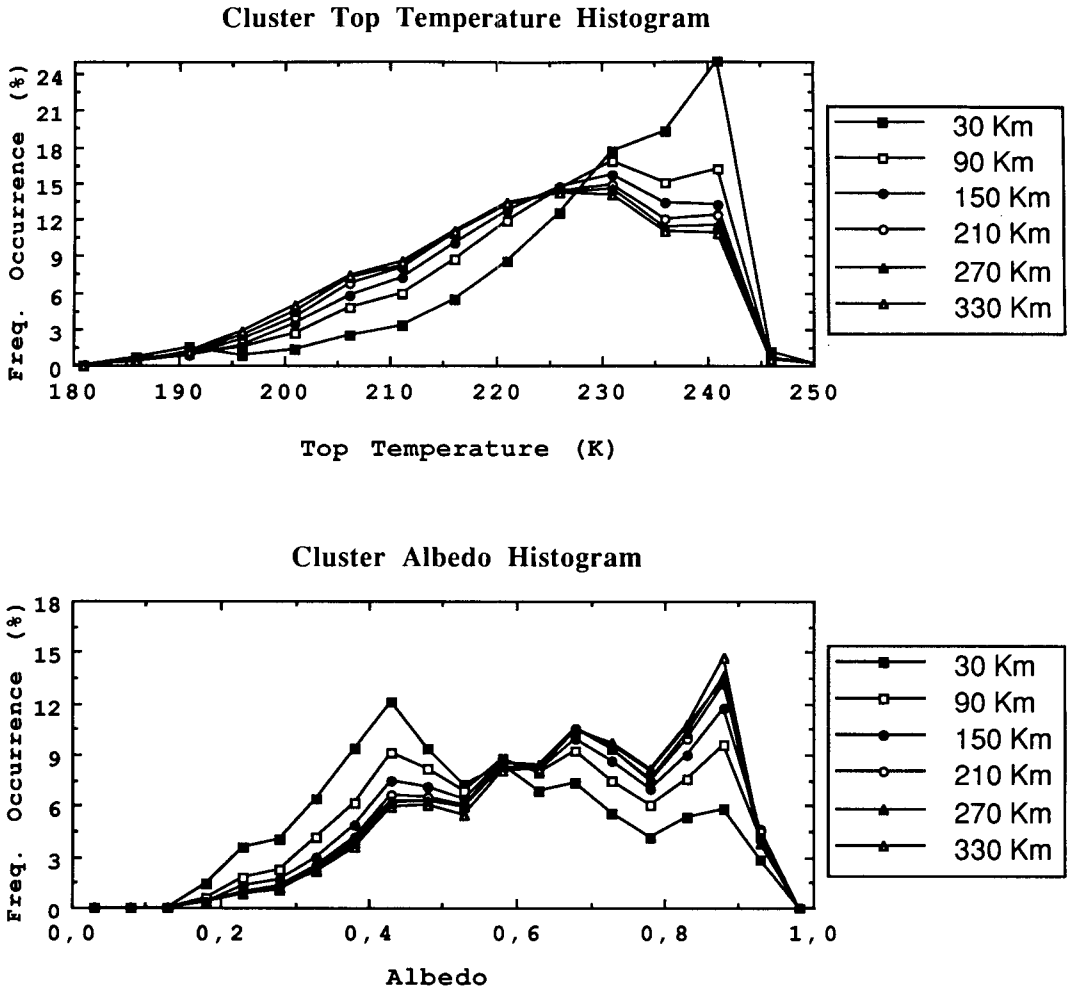

FIG. 4. Frequency distribution of (a) cloud-top temperatures and (b) cloud visible albedos for individual image pixels within convective cloud clusters of different radii. Results for local noontime images aggregated over January–February and July–August 1987 and 1988.

cells (cf. Fu et al. 1990). The smallest maximum (ALB near 0.40) generally comprises clouds that have TC values in the range 225–245 K, whereas the clouds with ALB near 0.65 have TC values in the range 215–235 K. We identify these two as thinner and thicker portions of the MAC, respectively, and refer to the thinner part as the CAC and the thicker part as the TAC.[1] Fu et al. (1990) identified cirrus anvil clouds with 215 K < TC < 267 K. Figure 4b also shows that the relative proportion of the three components is nearly constant for all sizes of CS except the smallest. In the smallest CS, the population of clouds with ALB values near the low ALB maximum is much larger than that at the other two maxima. Figure 5 shows a schematic of different types of CS and their subdivision into component cloud types; the following discussion summarizes additional evidence for this model.

We can clarify the nature of the smallest CS with Figs. 6, 7, and 8. Figure 6 shows the probability at different local times for each size range of CS over land and ocean to contain at least one pixel with the cloud properties of a convective cell. To obtain a result that takes proper account of diurnal variations, this analysis uses only a TC threshold (TC < 215 K) at each local time of day (Figs. 6 and 8) to identify the convective regions (cf. Fu et al. 1990). Only about 10% of the smallest CS (<60 km) have at least one Cb within them for any time of the day, whereas more than 60% of the medium and large CS over ocean and more than 80% over land have at least one Cb. Thus, the smaller CS are predominantly systems with no active convective

[1] We use this name to indicate that this category is difficult to separate uniquely from the cirrus and convective components; however, we believe it to be significant because the relative proportion of this cloud type varies systematically with CS size.

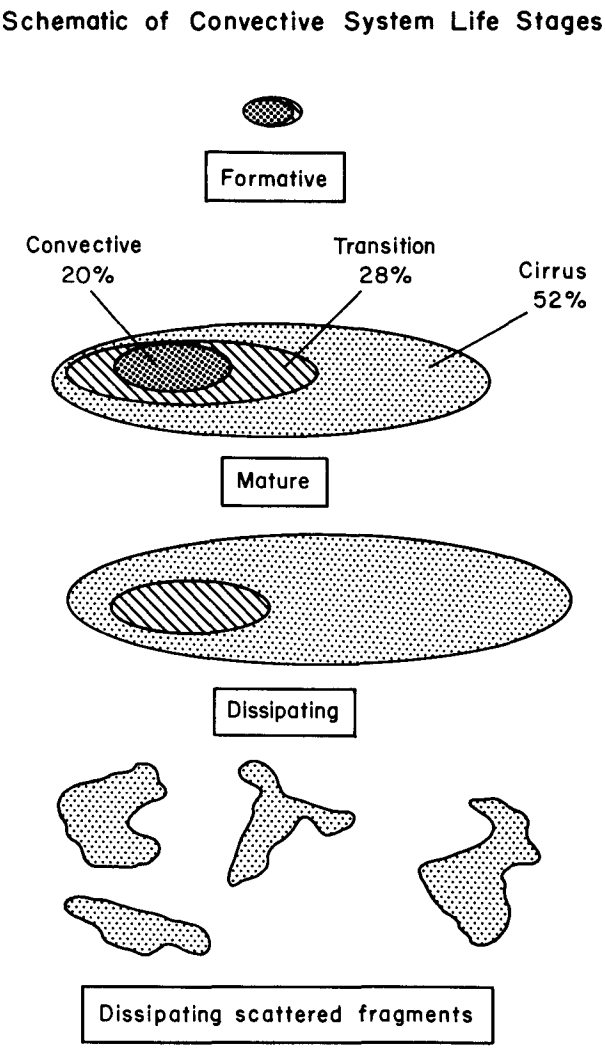

FIG. 5. Schematic cloud structure in an average tropical convective system in its formative, mature, and dissipating stages, illustrating terminology used in text.

cells apparent, whereas the medium and large CS are predominantly convectively active.

In Fig. 7 we plot the frequency distribution of the fraction of the total CS area covered by Cb clouds (Fig. 7a) and the fraction covered by Cb and TAC, together (Fig. 7b), as a function of the size of the total CS. In this figure we use an albedo threshold (ALB = 0.70) in noontime images to separate the Cb and TAC parts, both of which have TC < 245 K. Figure 7 includes only those CS containing at least one Cb. The distribution shapes show that the smallest CS containing Cb differ[2] from all the other CS containing Cb in that about 25%–65% of their total area is occupied by Cb (Fig. 7a) with little TAC evident. (Combining Cb and TAC in Fig. 7b does not change the distribution shape.) All of the larger-sized CS exhibit the same distribution shape, where the Cb fractional area is below about 30% and the Cb + TAC fractional area is between 25% and 75%. Thus, we conclude that the smallest CS are of two different types, one with no convective activity apparent and one that appears to be the combination of Cb and some CAC. The medium and large CS (there are around 20% of these without deep convection) are generally one type of system with the same proportions of Cb, TAC, and CAC.

The medium and large CS that do not show any convective activity, particularly over oceans, may be produced partly by the application of a specific ALB threshold to identify Cb (and separate TAC from CAC). We have used the features in Fig. 4b to define these thresholds, but Fig. 7 suggests that the Cb and TAC fractions occupy nearly constant proportions

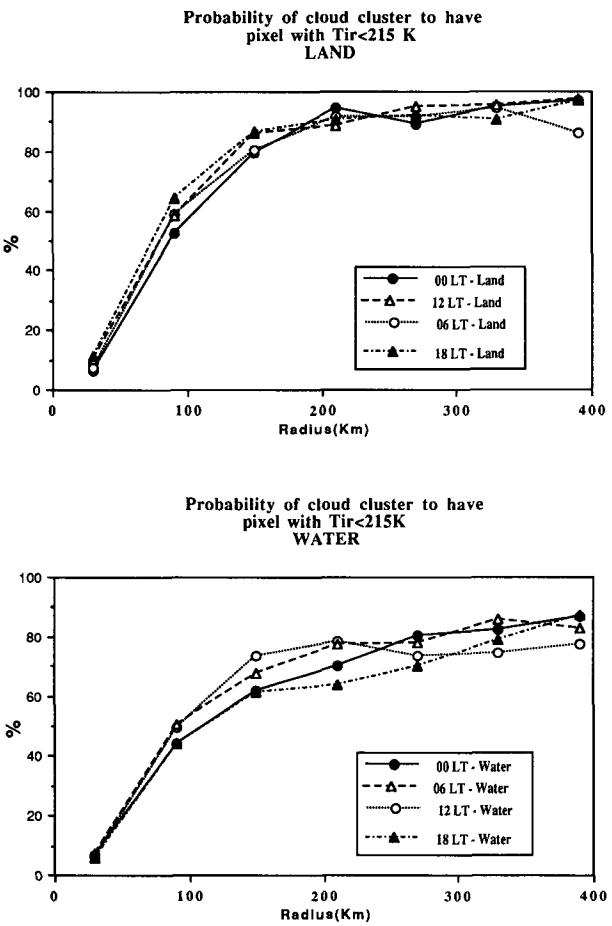

FIG. 6. Average probability at each local time that convective cloud clusters in July 1988 over (a) land and (b) ocean contain at least one image pixel with cloud-top temperature less than 215 K as a function of cloud cluster radius.

[2] The large variations between frequency peaks for the smallest CS in Fig. 7 arises from the effects of the small number (approximately 3–10) of pixels composing the CS in this category.

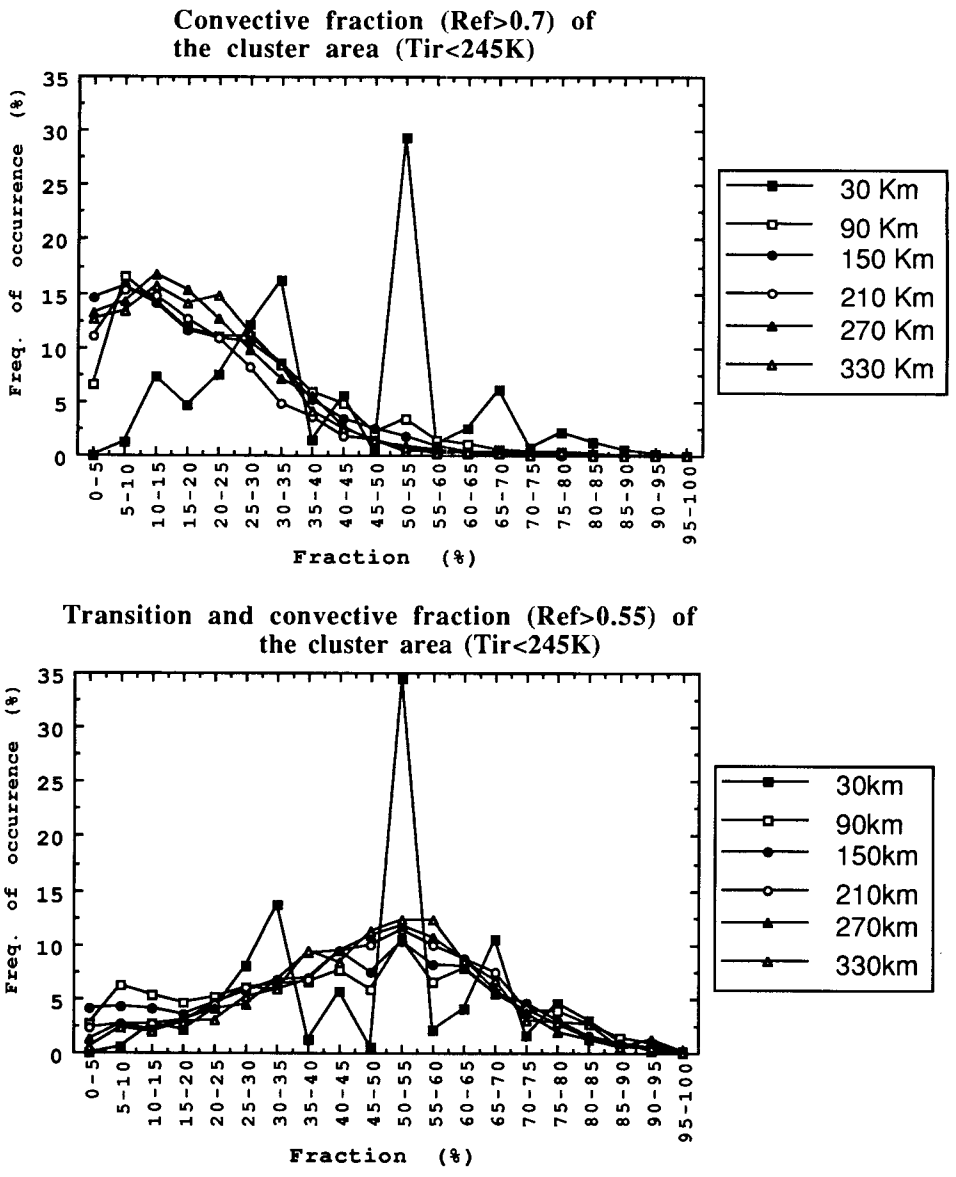

FIG. 7. Frequency distribution at noontime for 1987–88 of the fraction of cloud cluster area occupied by clouds with top temperatures less than 245 K and (a) albedo greater than 0.7 and (b) albedo greater than 0.55 as a function of cloud cluster radius.

of all CS except the smallest, so that distinguishing them is difficult (hence our use of the name "transition anvil" cloud). If we lower the ALB threshold separating Cb and TAC to 0.6 (including much of the TAC clouds in the Cb category), then land–ocean differences nearly disappear, since almost all CS > 180 km contain at least one Cb defined by this lower threshold. We note that this behavior of the results does indicate a systematic difference between the "thicker" portions of land and ocean CS. We return to this discussion when considering the diurnal variations of CS.

Thus, the majority of larger CS are convectively active systems that are composed, on average, of about the same proportions of Cb, TAC, and CAC (Fig. 5); but note that Fig. 7 indicates that the variations of these proportions among individual CS are quite large. It is only in the average sense that the structure of the CS can be described as constant with size. Figure 8 shows the average areal fraction of the larger CS over land and ocean that is occupied by the convective cells, separated by local time: it is nearly constant with CS size and is about 5% smaller for ocean CS than for land CS on average. The nearly constant fraction of Cb

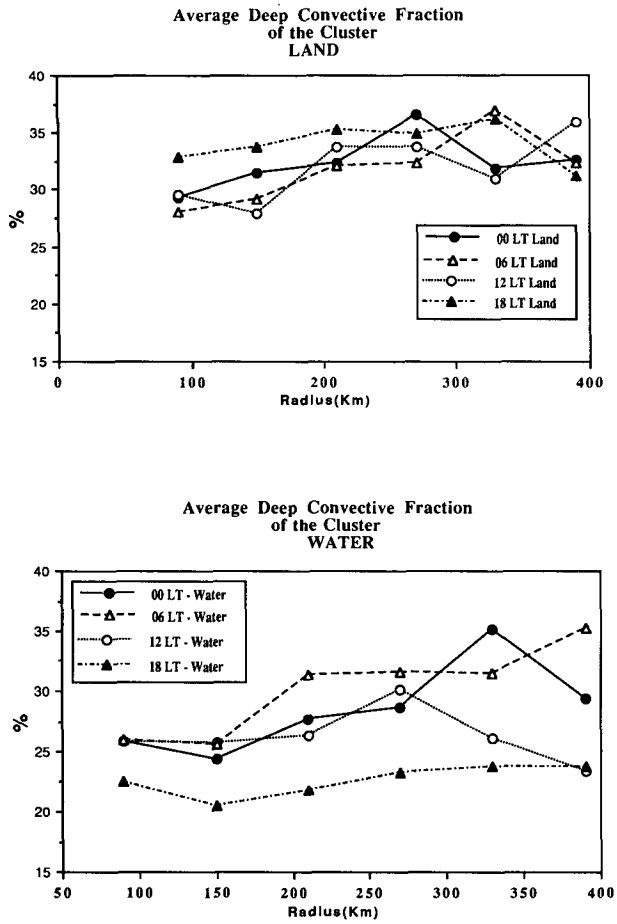

FIG. 8. Average fraction in July 1988 at each local time of the cloud cluster area occupied by clouds with top temperatures less than 215 K as a function of cloud cluster radius over (a) land and (b) ocean.

means that the area covered by MAC, representing about 75%–80% of the total CS area, and the whole CS area are both proportional to the Cb area. Even the partitioning of the anvil cloud into the thicker and thinner parts appears to be constant with the size of the total system.

2) AVERAGE CLOUD PROPERTIES

We analyze the noontime images to obtain average cloud properties for the whole CS and for the Cb and MAC components, separately. Our analysis is applied to CS having sizes smaller than the "break radius" (360 km in Fig. 2) in order to have about the same pixel population in each size class over the whole range. In the figures that follow, we show cloud properties averaged over CS in a size class; however, the variations of the cloud properties of individual CS within a size class are larger than the differences between the average properties of adjacent size classes, though of similar magnitude at all sizes. The variations of TC (ALB) are generally smaller than (similar to) the variations of average values among individual CS. The standard deviations for TC and ALB for the whole dataset are 14 K and 0.16, but are reduced by about a factor of 2 if only CS in one season in the same year over one surface type (land or ocean) are considered.

Figure 9 shows the variation of TC with size for the Cb part, the MAC part, and the whole CS. The values shown represent the average over all image pixels as-

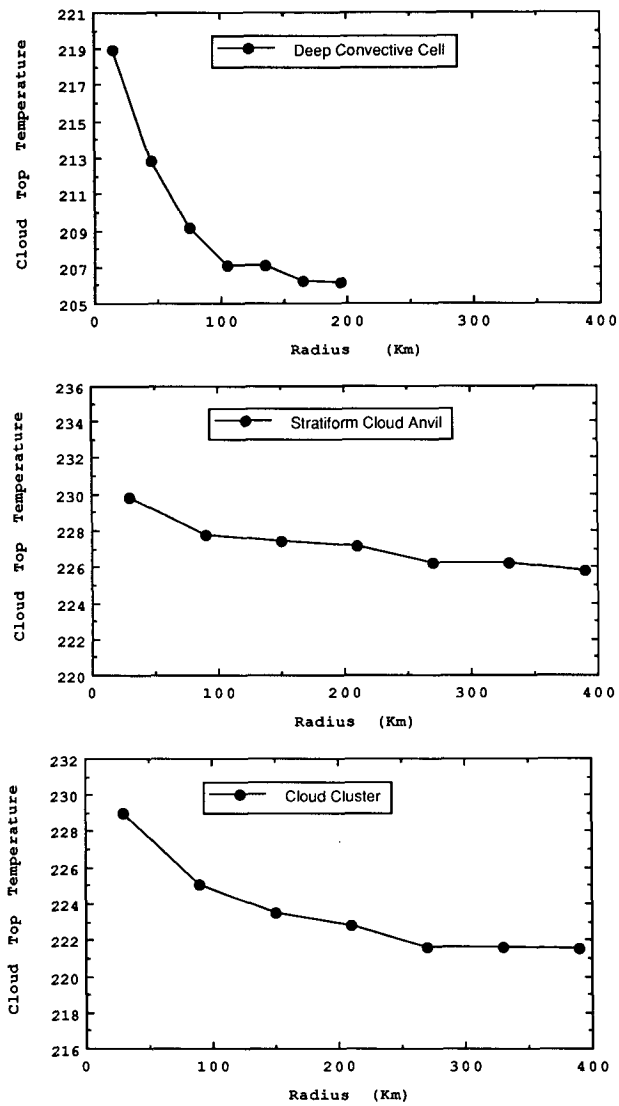

FIG. 9. Variation of average cloud-top temperatures with size (radius) of (a) all convective cells within convective systems (cloud-top temperature less than 245 K, cloud albedo greater than 0.7), (b) the anvil cloud parts of convective systems (cloud-top temperature less than 245 K, cloud albedo less than 0.7), and (c) the whole convective system. Results are for local noontime images aggregated over January–February and July–August 1987 and 1988.

sociated with the same class size interval without regard to their location and distribution within individual CS. The size analysis for the Cb, which is performed separately from the whole CS size analysis, shows a variation of TC from 219 K for the smallest Cb (≤30 km) to 206 K for the largest Cb (greater than 100 km, which are systems with many Cbs), corresponding to a cloud-top pressure variation of about 55 mb. This systematic increase of cloud-top height with horizontal size of the Cb (also in Machado et al. 1992) is consistent with other studies that show a positive correlation between convective vertical velocity and convective core horizontal size (e.g., Zipser and LeMone 1980) and convective cloud-top height (e.g., Betts 1973). In contrast to the convective part, the mesoscale anvil TC does not vary strongly with size (Fig. 9b); the average anvil cloud has almost the same TC of about 228 K, regardless of size. This temperature corresponds to a cloud-top pressure of about 250 mb, which coincides with the top of the stratiform anvil convergence layer (Gamache and Houze 1982). Tollerud and Esbensen (1985), by composite analysis of GATE data, show that the divergence at higher levels varies in strength among the different development stages of a CS but remains at about the same height throughout its lifetime.

Since the majority of the area of the whole CS is composed of anvil cloud, the average value of TC for the whole CS exhibits only a small variation with the size, from 229 K for small systems to 222 K for larger ones (Fig. 9c). However, this result is actually produced by two related features: the larger Cb with colder tops are preferentially formed in larger CS, and the probability of Cb occurrence is larger in the larger CS.

The average albedo for the Cb is nearly the same for all sizes (Fig. 10a), because these clouds are already so optically thick that the reflection of shortwave radiation is very insensitive to any further changes in optical thickness. (Note, however, that even a 1% change in albedo at these values represents about a 10% change in cloud water content.) In contrast, the MAC albedo varies with the size (Fig. 10b). The variation between the smallest and the largest MAC is associated with an increasing proportion of the thicker TAC in the presence of active convective cells: the smaller CS mostly lack Cb and TAC (Fig. 7). Webster and Houze (1991), describing the EMEX project, refer to the cloud clusters as having a convective–transition pattern, where the transition parts correspond to the convective cells that are undergoing a transition from actively convective to stratiform structure. Old convective cells merge into the anvil, supplying it with ice particles and momentum (Houze 1977). Regions with larger ice–water contents are probably the anvil regions that produce the bulk of the stratiform rain. The average albedo distribution for the whole CS (Fig. 10c) also varies with size because the probability of a given CS size to have Cb increases with size (Fig. 6).

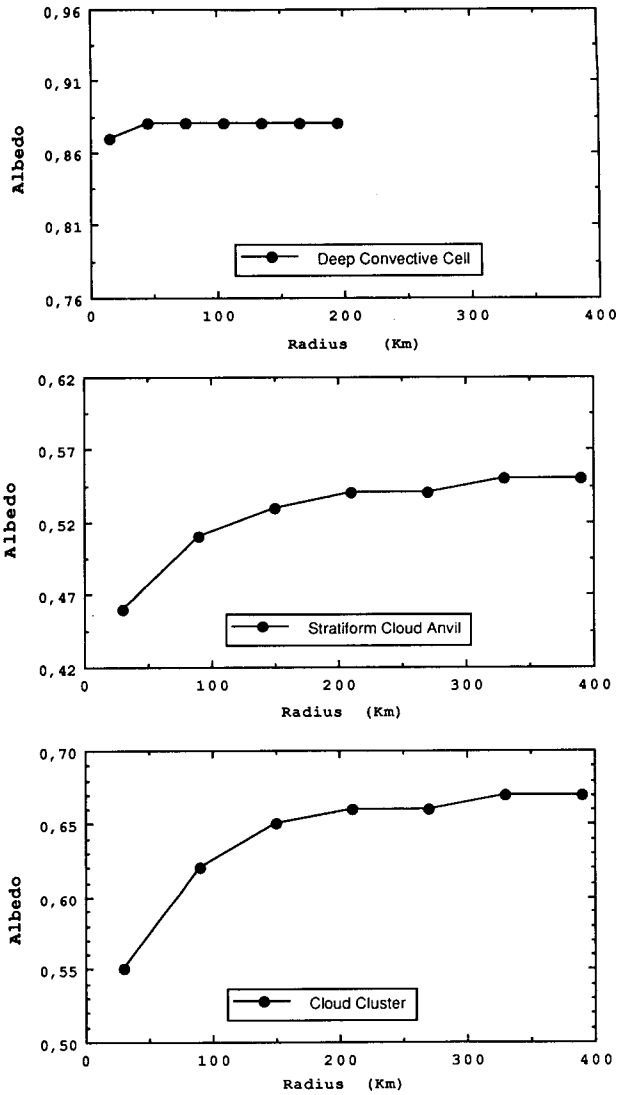

FIG. 10. Same as Fig. 9 but for average cloud albedos.

3) SEASONAL AND INTERANNUAL VARIATIONS

Figures 11 and 12 compare the variations of TC and ALB, respectively, with CS sizes between land and water, between Jul–Aug and Jan–Feb (changes associated with shifting geographical distribution) and between an El Niño (1987) and a La Niña (1988) year. These results are averaged over all CS, regardless of whether they contain Cb. Some differences occur among the different satellite regions, principally between the Pacific and Atlantic–Africa sectors; however, the most important differences are between land and ocean CS properties. Over ocean the variation of the cloud properties with size (Figs. 11a and 12a) is larger than over land. The smaller CS over land have colder TC than over ocean, while the larger CS have about the same TC over both land and ocean. The smaller CS over land have larger ALB values than over ocean, but the

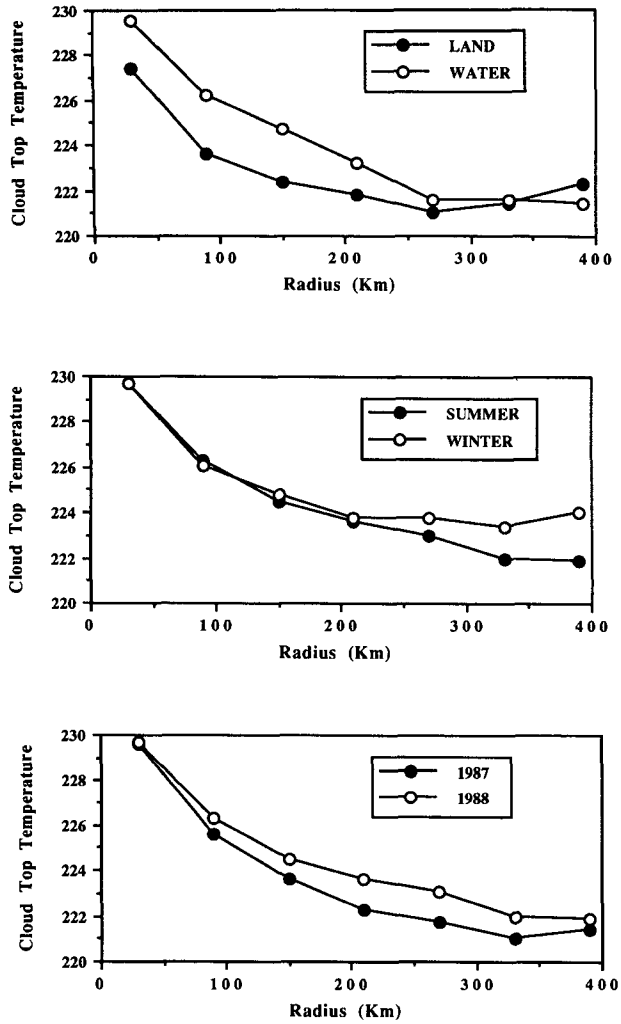

FIG. 11. Variations of average cloud-top temperatures with radius of the convective system (a) for land and ocean averaged over both seasons and years, (b) for January–February and July–August averaged over land and ocean and both years, and (c) for 1987 and 1988 averaged over land and ocean and both seasons.

ALB values for ocean CS increase much more with size than over land, so that the larger ocean CS have higher ALB values.

Figure 11b shows that the average TC values in Jul–Aug and Jan–Feb are nearly the same for all but the largest CS, which have slightly higher tops in Jul–Aug. In contrast, ALB values are larger in Jul–Aug for all CS sizes (Fig. 12b), which is explained by the changing proportion of land and ocean CS in the two seasons and the higher ALB values for ocean CS. El Niño conditions appear to decrease TC (increase cloud-top heights) for larger CS (Fig. 11c) and decrease the ALB values for the smaller CS (Fig. 12c) relative to La Niña conditions. These small differences are observed mainly in the Pacific sector and may be associated with the shift of some convective activity away from islands into the open ocean.

4) LAND–OCEAN DIFFERENCES IN CS

As with the CS size distributions, the most important differences in the cloud properties are between land and ocean CS (Figs. 3, 11, and 12). We examine these differences in more detail because Fig. 12 presents a puzzle. A number of studies have noted that convective updrafts are much stronger over land than ocean (e.g., Jorgensen and LeMone 1989; Takahashi 1990), and since updraft strength is positively correlated with cloud-top height (Zipser and LeMone 1980), horizontal size (Betts 1973), and rainfall rate (Leary 1984), we might expect that CS over land would have lower TC and higher ALB (higher water contents) than CS over ocean. While the TC values for land CS (Fig. 11a) meet our expectation, the ALB values do not for large

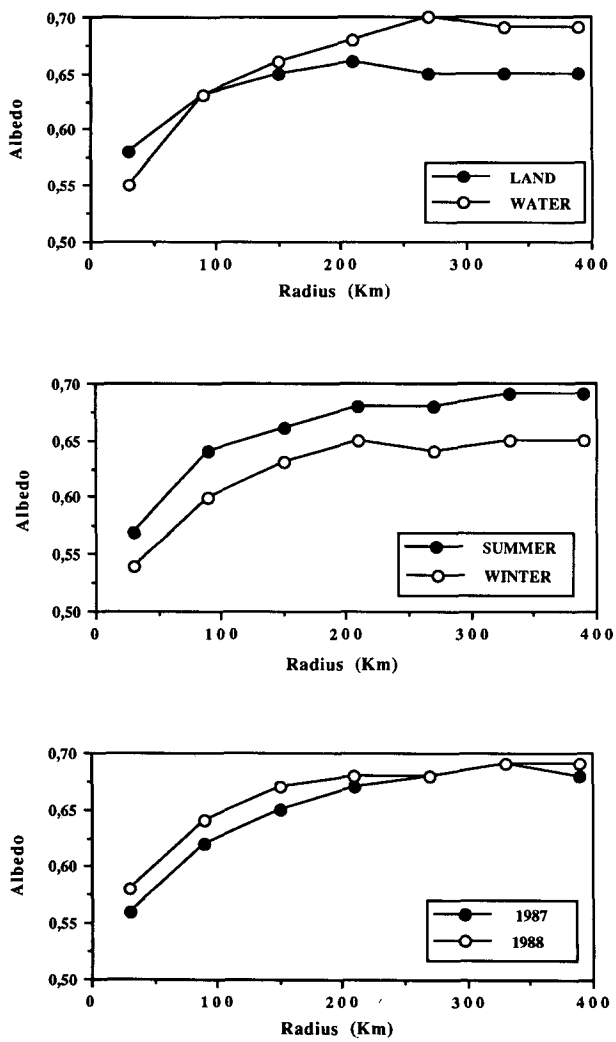

FIG. 12. Same as Fig. 11 but for average cloud albedos.

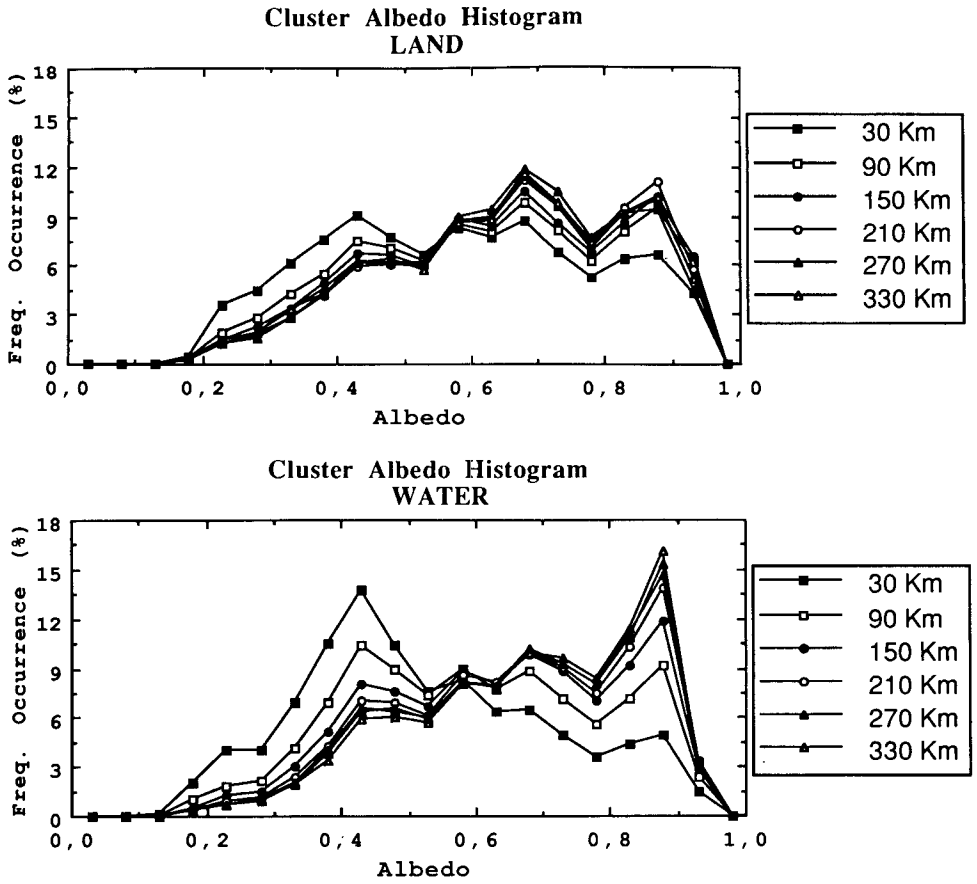

FIG. 13. Same as Fig. 4b but separated into land and ocean convective systems.

CS (Fig. 12a). However, these figures average results from both seasons, which involves changes in geographic location of the CS. Examination of individual seasonal results shows that land CS in the smallest three size categories, indeed, have higher albedos than over oceans. In addition, when we isolate the Cb and average their properties without regard to their location within CS of varying sizes, we find that land Cb have TC values that are about 3 K lower (higher tops) and ALB values that are about 2% higher than ocean Cb, consistent with the generally stronger convective updrafts observed in land convection compared with ocean convection (Jorgensen and LeMone 1989; Takahashi 1990). Stephens and Greenwald (1991) suggest similar systematic differences in CS properties from analysis of differences in radiation budget measurements. These results are also consistent with the change in partitioning between the convective and transition anvil portions of CS when we change the ALB threshold between them, which implies that there is more "intermediate"-ALB cloud present in ocean CS than land CS. Although the ALB difference may not seem significant, it does represent about a 25% increase in cloud water path going from ocean to land clouds. Moreover, since we are examining the land Cb at the time of minimum areal coverage (1200 LST) by this cloud type (e.g., Machado et al. 1993), the daily average ALB of land Cb is probably higher than shown in our results (however, our result as it stands is more relevant for determining the radiative effects of CS). So at least the convective part of the CS exhibits the expected colder TC (higher tops) and higher ALB over land than over ocean.

To understand whether these results are consistent with other studies and why the larger CS over land have lower ALB values than ocean CS, we separate the frequency distribution of ALB values from individual image pixels, shown in Fig. 4b, into its land and ocean parts at noontime (Fig. 13). The land and ocean CS exhibit distributions of TC that are very similar to that shown in Fig. 4a, but their ALB distributions are distinctly different. Figure 13 shows that the differences in average ALB for land and ocean Cb are associated with different distribution shapes: there is a significantly higher relative population of Cb with $0.90 < \text{ALB} < 0.95$ over land than ocean, even though we are observing the land Cb near the time (1200 LST) of their minimum areal coverage (Machado et al. 1993). Also, we can see that the differences between the TC and ALB values of the smaller CS have much more to do

with the fact that a larger fraction of these systems contain Cb over land than over ocean than with differences in the average values of TC and ALB for Cb. This difference in the relative fraction of Cb occurs despite the fact that the land convection is at its daily minimum areal coverage while the ocean convection is near its daily average coverage.

The differences in average properties of the larger CS over land and ocean are caused by more complex variations in structure. The most notable differences are that land CS have a relatively larger proportion of TAC and less Cb than ocean CS; however, at least the Cb difference is probably a direct consequence of using local noontime images to construct Fig. 13. The daily average fraction of Cb in land CS is actually larger than in ocean CS (Fig. 7); however, the Cb over land is a minimum at local noon and is near its daily average value over ocean (Machado et al. 1992). We cannot tell whether the anvil clouds undergo a significant diurnal cycle as well, though some studies have indicated that the diurnal variability of the anvil clouds is much less than that of the Cb clouds (Fu et al. 1990; Miller and Fritsch 1991; Machado et al. 1993—also see discussion in section 4b). In any case, at the noontime minimum of convective activity over land, our simple ALB threshold may mistake "inactive" convection for TAC. Thus, at noontime, the larger ALB values of the larger ocean CS may be caused by a larger relative contribution by Cb at that time of day.

5) DIURNAL VARIATIONS

The diurnal cycle of clouds is one of the most important features of tropical variability over both land and ocean—for example, in the Atlantic and Africa sectors (e.g., Minnis and Harrison 1984; Duvel 1989). The convective parts of the larger CS over both land and ocean undergo significant diurnal variations with different phases (Miller and Fritsch 1991; Machado et al. 1993); however, only the large CS over ocean exhibit a diurnal variation of the mesoscale anvil cloud component with a smaller amplitude and different phase than the convective part (Fu et al. 1990; Machado et al. 1992).

Figure 6a shows that the probability of a CS over land containing at least one image pixel identified as Cb varies little over the diurnal cycle, despite a clear diurnal variation of the Cb amount over land with a maximum in late afternoon. There is, however, a weak indication that medium CS are more likely to contain Cb at 1800 LST and that large CS are less likely to contain Cb at 0600 LST (Fig. 6a). The CS over ocean (Fig. 6b) exhibit slightly more variation of this probability with diurnal phase, with Cb more likely at 0600–1200 LST for medium CS and less likely at 1200 LST for larger CS (Fig. 7b). The fractional area occupied by the Cb shows a similar behavior. Both of these variations could partly be the consequence of the smaller optical thicknesses of ocean Cb, compared to land Cb, implied by the changed portions inferred with a different ALB threshold. Smaller CS over land (<240 km) show larger Cb fraction at 1800 LST, whereas larger CS do not show any simple diurnal variation (Fig. 8a). Over ocean (Fig. 8b) the Cb fraction is clearly a minimum at 1800 LST for all sizes of CS and at a maximum at 0600 LST for almost all sizes.

4. Radiative effects of CS

We evaluate the radiative effects of the CS using their average cloud properties and structure. These results are not new (e.g., Chen and Cotton 1988), but we emphasize the implications of CS variations with size, time of day, and location. We separate all CS into three sizes: small ($R \leq 180$ km), medium ($180 < R \leq 360$ km), and large ($R > 360$ km). The area of an average CS is divided into three parts: 20% Cb, 28% TAC, and 52% CAC. The average optical properties of these three cloud types are for Cb, PC = 208 mb, PB = 900 mb, and TAU = 65; for TAC, PC = 262 mb, PB = 600 mb, and TAU = 23; and for CAC, PC = 262 mb, PB = 600 mb, and TAU = 5.

a. Local effects

Using the average of the CS cloud properties shown in Figs. 8, 9, and 10, we calculate the daily average changes in the radiative fluxes at the top of the atmosphere and at the surface caused by adding 100% CS cloud cover. The effects of the diurnal variation of ocean surface albedo with solar zenith angle and of the surface temperature diurnal variation are included, but we hold the cloud properties constant over the whole diurnal cycle. Table 1 summarizes the effects for cloud properties averaged over all CS, as well as for the separate parts of CS clouds. Figure 14 illustrates the changes in net flux at the top of the atmosphere for the three size ranges of CS over land and ocean; these results are for noontime when the decrease in solar heating (solar—SW) is largest. The change in total net flux ranges from about -300 to -450 W m^{-2}, a strong cooling. The changes in net terrestrial fluxes (LW) at the top of the atmosphere, which are the changes in total net flux at night, range from about $+100$ to $+140$ W m^{-2}, a weaker heating. Thus, the changes in net SW fluxes range from about -450 to -600 W m^{-2}. In other words, the variation with CS size of the effects on the net fluxes during the daytime results from two opposing changes: smaller (larger) CS have higher (lower) cloud-top temperatures—implying more (less) LW cooling—and lower (higher) albedos—implying more (less) SW heating. At night the larger CS allow less cooling than smaller CS.

The relative importance of the Cb and MACs can be estimated from the differences between the net flux changes produced by the whole CS (called the "clus-

TABLE 1. Summary of the daily average net radiative effects of 100% cloud cover for average convective cloud properties, as well as the separate effects of 100% cover by average convective cell clouds, transition anvil clouds, cirrus anvil clouds, and total anvil clouds. To get the total anvil values from the transition and cirrus parts, weights of 0.35 and 0.65, respectively, are used. To get the total CS values from convective and total anvil parts, weights of 0.20 and 0.80, respectively, are used. Net flux changes are calculated with constant cloud properties and annual mean conditions and are shown for the surface, atmosphere, and top of atmosphere in watts per square meter.

		Change in net radiative fluxes ($W\ m^{-2}$)		
Region	Cloud type	Surface	Atmosphere	Top
Land	CS	−133	+98	−35
	Convective	−188	+71	−118
	Mesoscale anvil	−119	+104	−14
	Transition anvil	−164	+92	−71
	Cirrus anvil	−95	+111	+16
Ocean	CS	−160	+96	−64
	Convective	−218	+65	−153
	Mesoscale anvil	−146	+104	−41
	Transition anvil	−197	+92	+105
	Cirrus anvil	−118	+111	−7

ter") and the anvil parts alone (Table 1 and Fig. 14). Adding Cb clouds to the anvil clouds decreases the daily mean net radiative flux (a cooling effect) by about 20–50 $W\ m^{-2}$, but the effect on the net SW flux is actually about twice as large. Adding Cb clouds at night increases the net flux (a heating effect) by about 20–50 $W\ m^{-2}$. Thus, the larger ALB of the Cbs (Fig. 10) is somewhat more important to the radiative effect of the whole CS than their colder TC values (Fig. 9), but both effects are significant. The presence of Cb, if constant over the day, moderates the diurnal flux variations; the differing diurnal variations of Cb over land and ocean decrease and increase their moderating influence, respectively. We note that the difference in magnitude of the fluxes among the different-sized CS is similar in magnitude to the effect of adding Cb clouds to the MACs.

The net flux change caused by CS over ocean is larger in magnitude (stronger cooling effect) than over land. Although some of this difference is associated with differences between the characteristics of land and ocean CS (Figs. 11 and 12), the most important effect is that larger surface albedos over land reduce the SW cloud effect. A small difference in average TC between ocean and land CS (land TC less than ocean TC) is reinforced by an opposite, small difference in the average ocean and land surface temperatures (land TS greater than ocean TS), making the change of net LW flux caused by CS larger over land than ocean. Thus, the changes in net fluxes caused by CS are reduced in daytime and enhanced at night over land relative to CS over oceans.

At the surface the changes in net SW fluxes produced by the CS are very similar in magnitude to those at the top of the atmosphere, since atmospheric absorption is typically only about 15–25 $W\ m^{-2}$ (slightly larger over the higher albedo land areas). The changes in the net LW fluxes at the surface are, however, only about 30%–40% of the changes at the top of the atmosphere because of the large infrared opacity of water vapor in the tropical atmosphere. Thus, the effect of CS on the surface net flux is larger (stronger cooling) than their effect on the net flux at the top of the atmosphere during daytime and smaller than their effect on the net flux at the top of the atmosphere during nighttime.

Figures 15, 16, and 17 show vertical profiles of the radiative heating–cooling rates at noontime calculated for the medium-sized CS; Figs. 15 and 16 show the separate effects of the Cb and MAC, and Fig. 17 shows

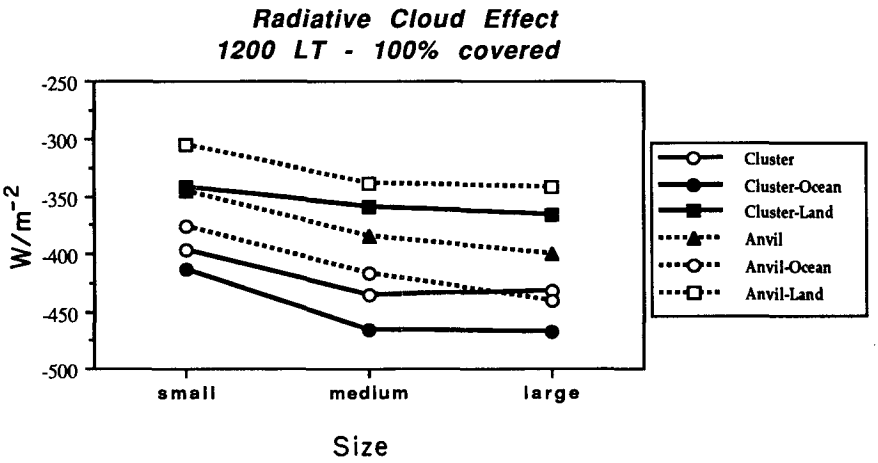

FIG. 14. Average change in net radiative flux at the top of the atmosphere at noontime from clear tropical conditions produced by 100% cover by small ($0 < R < 180$ km), medium ($180 < R < 360$ km), and large ($R > 360$ km) convective systems and by the anvil part of these convective systems over land and ocean.

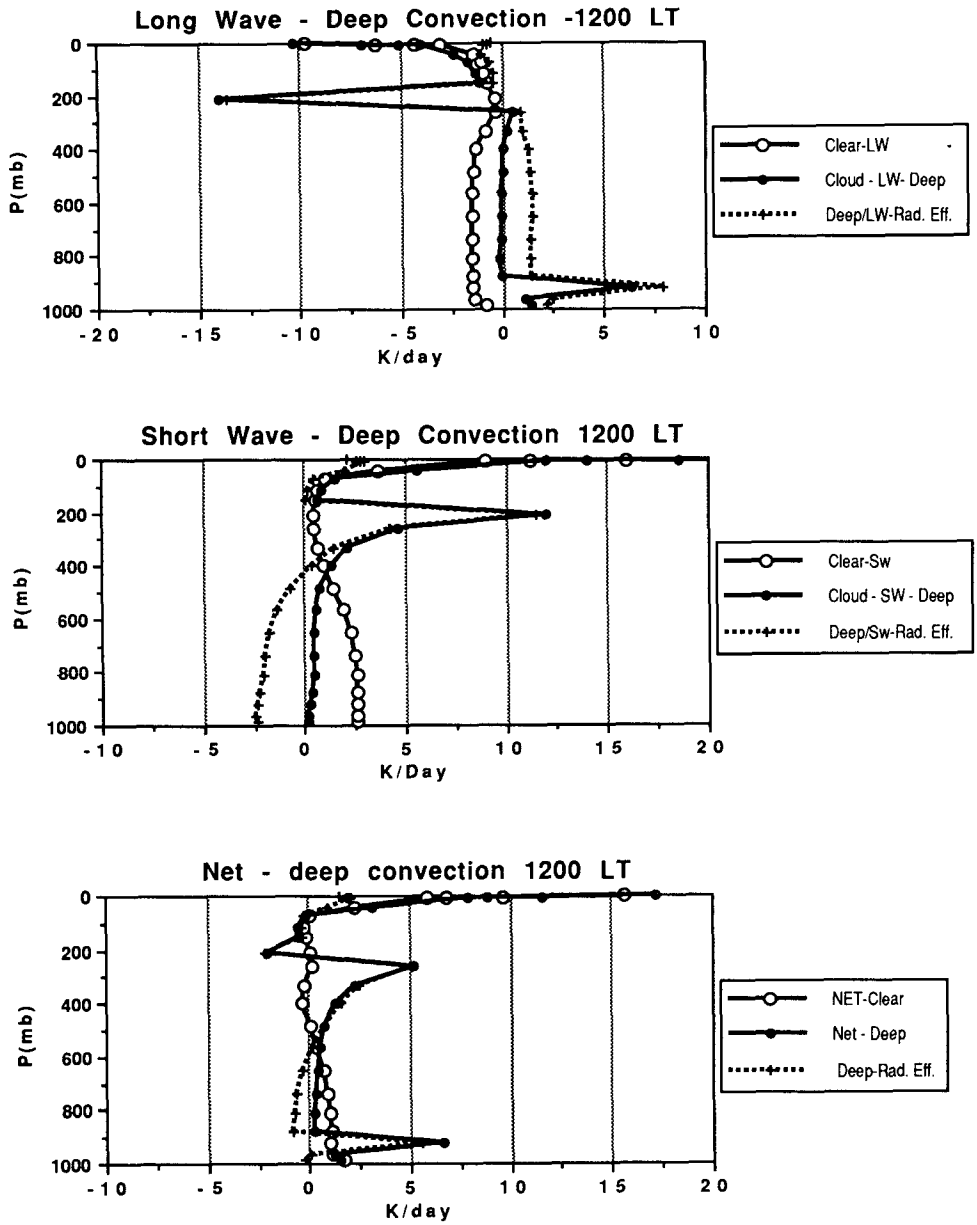

FIG. 15. Vertical profile of radiative heating–cooling rates for the convective cell component of medium-sized (180–360 km) convective systems, based on average cloud properties. Each panel shows the clear sky, the cloudy sky (100% cloud cover), and the difference for (a) longwave, (b) shortwave, and (c) net heating–cooling rates. The heating–cooling rates are calculated for noontime with an annual average solar flux for the tropics.

the effects of the whole CS, which is a weighted average of the Cb and MAC effects. The results for the whole CS agree well with other diagnoses of the radiative effects of the clouds associated with CS (e.g., Stephens et al. 1978; Webster and Stephens 1980; Johnson and Young 1983; Houze 1989). The LW vertical flux profile does not change shape significantly during the day, so the LW results directly represent the nighttime net effect of the CS. The SW flux changes are much smaller when averaged over the daytime (by about a factor of 2) and smaller still when averaged over the whole day (another factor of 2).

Although the Cb radiative effects do not contribute much to the total effect of the larger CS, they have interesting implications for the convective dynamics of these systems and for the smaller CS systems that are composed mostly of Cb. The LW heating–cooling rates (Fig. 15a) imply a destabilization of the tropo-

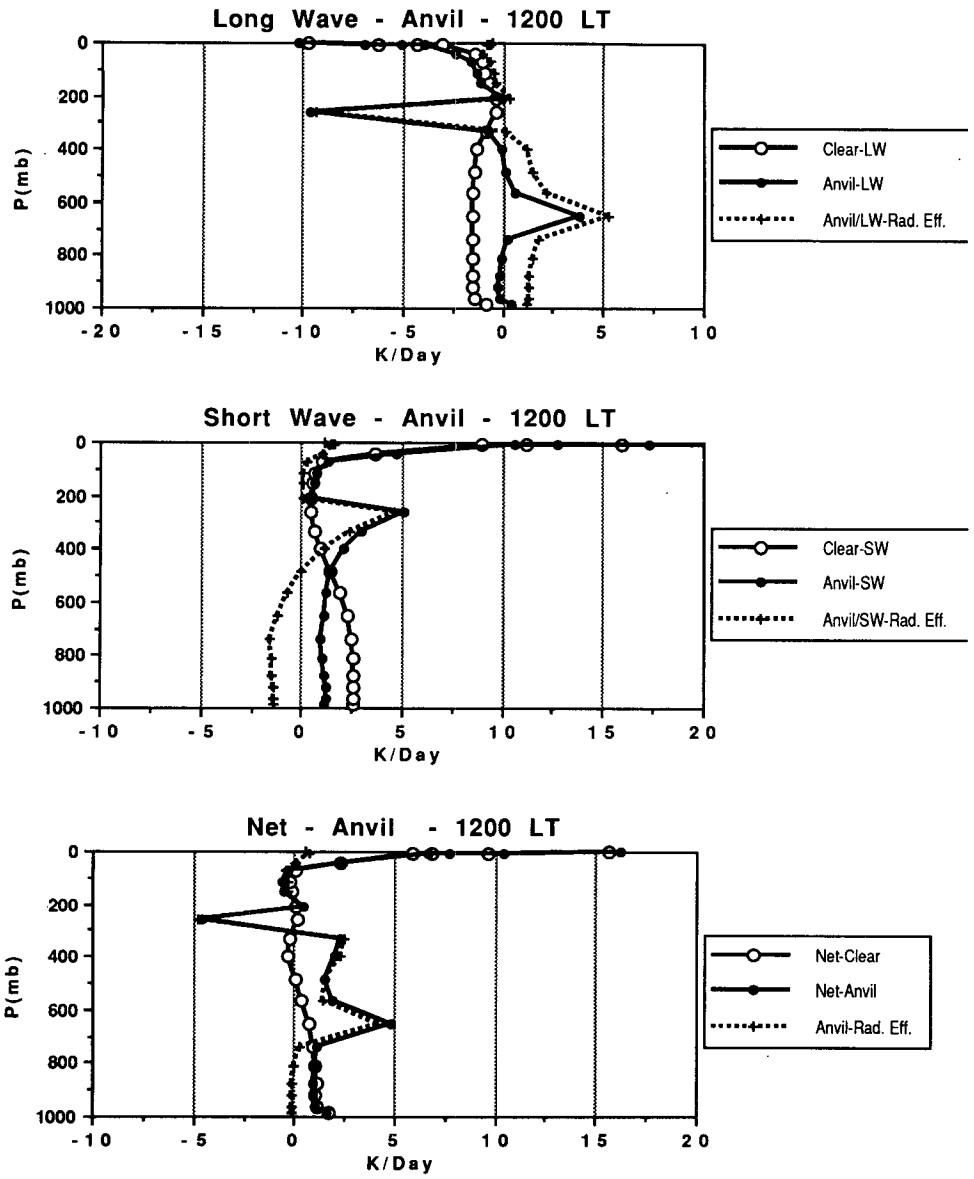

FIG. 16. Same as Fig. 15 but for the anvil cloud component of medium-sized (180–360 km) convective systems.

sphere by radiation at night (heating near the surface and cooling near the tropopause), but the heating near the top of the planetary boundary layer may actually cut off the convection if the atmospheric temperature can react to this net flux change over the short lifetime of Cbs. In other words, given the finite time required for the atmosphere to change temperature, the life cycle of the convection may be completed before the radiative effect stabilizes the lower atmosphere. Note that in the middle troposphere the Cb eliminates the clear-sky LW cooling. These two effects may help explain the tendency for more convection at night over oceans where diurnal variations of surface temperature are small. Gray and Jacobson (1977) explain a predawn maximum in convection by the radiative cooling rate contrast between the CS and the surroundings. During daytime, the tropospheric SW heating is concentrated near cloud top (Fig. 15b), which nearly cancels the LW cooling effect at noontime (Fig. 15c). However, since the SW heating and LW cooling occur at different levels near cloud top, a 100–200-mb layer is radiatively destabilized, even in the daily mean. The systematic decrease of TC with little change in ALB with increasing Cb size implies stronger destabilization in larger CS.

The MAC produces a similar vertical heating–cooling rate profile (Fig. 16) but with reduced magnitudes

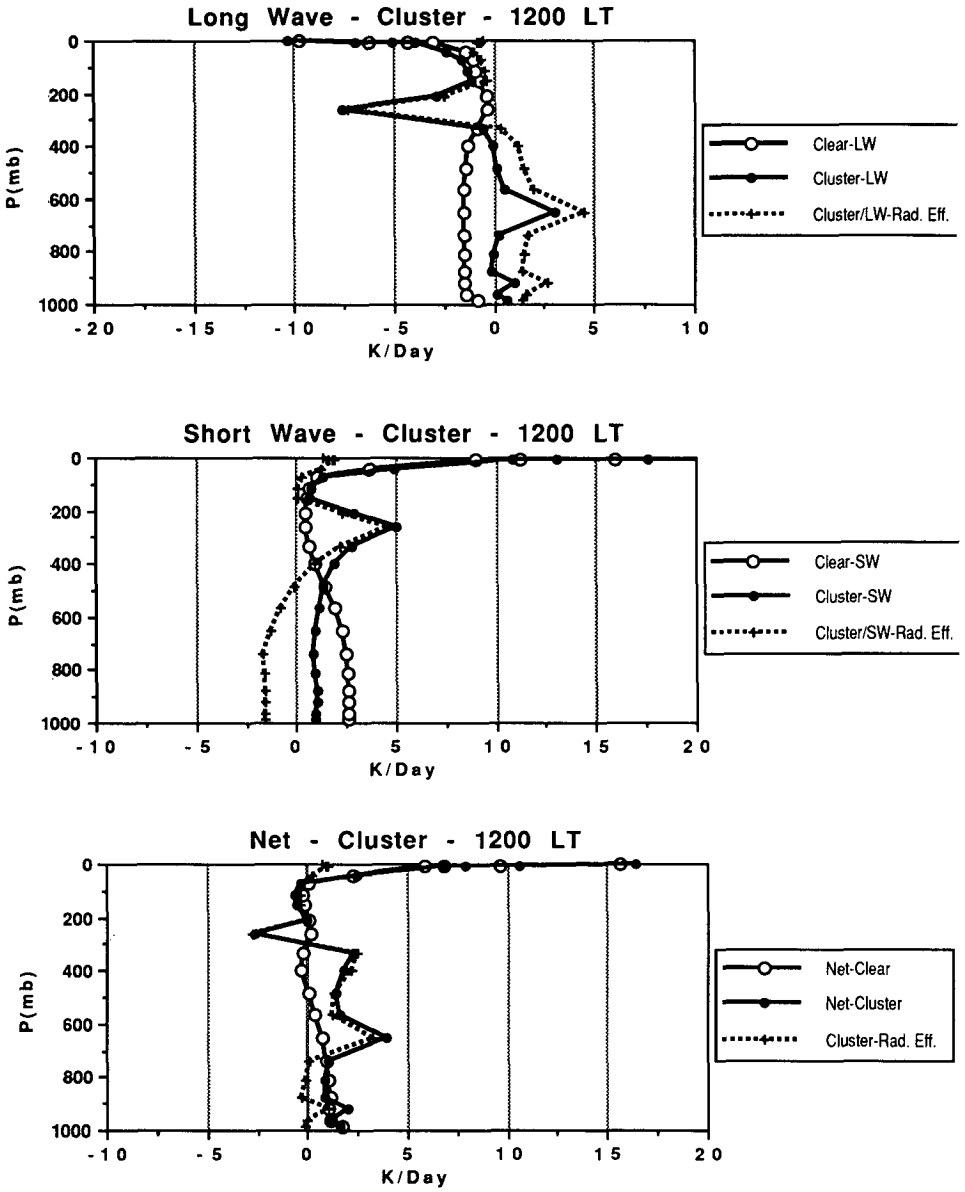

FIG. 17. Same as Fig. 15 but for the whole medium-sized (180–360 km) convective system. The heating–cooling rates for the convective cell and anvil clouds are weighted by 20% and 80%, respectively, representing their fractional area within the convective system.

and with the LW heating shifted to higher altitude (since cloud base is assumed to be at 600 mb). These changes are significant since, now, the MAC acts to destabilize the middle and upper troposphere both day and night, but more strongly at night. Since the anvil cloud dominates the total CS radiative effect, it is particularly significant that the total radiative heating–cooling rate profile (Fig. 17) acts to reinforce the mid-level warm core found in the larger CS, both day and night. However, as the size of CS increases, the MAC albedo increases, which decreases the net heating during daytime. At night over land, when the convective source of energy (heating) is diminished (Maddox 1983; Cotton et al. 1989; Miller and Fritsch 1991), such a radiative heating profile may help sustain the system. The magnitudes of these heating–cooling rates ($\approx$3–7 K day^{-1}) are about half the magnitudes of the estimated nonradiative (mostly latent) heating produced by the convective and stratiform components of CS (e.g., Esbensen et al. 1988; Houze 1989) and so cannot be considered to be dynamically insignificant.

Since the large CS have lifetimes of order 10–12 h (but many systems last more than 1 day) and their cloud properties undergo significant diurnal

changes, calculation of the daily average radiative effects of these clouds is more complicated than what we have done here. We defer discussion of this topic to section 5c.

b. *Large-scale effects*

As one estimate of the importance of CS in the radiation budget of the tropics, we calculate the changes in daily average net fluxes at the surface, in the atmosphere, and at the top of the atmosphere by weighting the results shown in Table 1 by the actual fractional coverage of CS and their component parts (Table 2). Again, we hold the cloud properties constant over the diurnal cycle. The cloud effect on the net SW fluxes at the top of the atmosphere is roughly twice the values shown in Table 2 because the cloud effect on net LW fluxes is almost the same in magnitude and opposite in sign. The changes in net LW are about a factor of 2–3 smaller at the surface than at the top of the atmosphere. Table 2 shows that the net effect of CS clouds at the top of the atmosphere, when averaged over the whole diurnal cycle with constant cloud properties, is very close to zero but still implies a small cooling. The net effect of CS at the surface is a larger cooling, which implies an overall tendency to stabilize the tropical atmosphere. Even though the convective cloud effect on the radiation budget of the tropics is very small on average, the spatial distribution of CS is not uniform, so that their radiative effects will play more of a role in tropical dynamics than suggested by these small numbers: the average patterns of tropical CS (Fig. 1) produce horizontal and vertical gradients in radiative heating and cooling that alter the mean circulation in both the zonal and meridional directions (cf. Sohn and Smith 1992).

TABLE 2. Summary of the daily average net radiative effects of average convective cloud systems on the whole tropics obtained by weighting results in Table 1 by actual cloud cover values for whole CS and for each cloud type, separately. To get total anvil and total cluster values, add the values for the component parts. Net flux changes are calculated with constant cloud properties and annual mean conditions and are shown for the surface, atmosphere, and top of the atmosphere in watts per square meter.

		Change in net radiative fluxes ($W\ m^{-2}$)		
Region	Cloud type	Surface	Atmosphere	Top
Land	CS	−11.3	+8.3	−3.0
	Convective	−3.2	+1.2	−2.0
	Mesoscale anvil	−8.1	+7.1	−1.0
	Transition anvil	−3.9	+2.2	−1.7
	Cirrus anvil	−4.2	+4.9	+0.7
Ocean	CS	−13.6	+8.2	−5.4
	Convective	−3.7	+1.1	−2.6
	Mesoscale anvil	−9.9	+7.1	−2.8
	Transition anvil	−4.7	+2.2	−2.5
	Cirrus anvil	−5.2	+4.9	−0.3

5. Discussion

a. *Implications of CS size distribution*

Numerous analyses of deep convection and mesoscale convective systems have produced many different classifications (cf. Cotton and Anthes 1989) that emphasize differences in their organization, evolution, and circulation regimes [e.g., squall lines, Houze (1977), non-squall lines, Tollerud and Esbensen (1985), and MCCs, Maddox (1980)]. Yet, a comparison of the results of these studies indicates a number of similarities in the cloud properties, structures, and energy budgets of all convective systems (cf. Houze and Hobbs 1982; Houze 1989; Cotton and Anthes 1989; Miller and Fritsch 1991).

Common features of the mesoscale forms of these systems are 1) a small subregion (about 20% of the total area, cf. Fig. 8) within the system encompassing the strongest updrafts and downdrafts that have dense clouds extending from near the top of the planetary boundary layer to near the tropopause and produce the peak intensity of precipitation, and 2) a larger region covered by a stratiform cloud, with a base located in the middle troposphere, that is responsible for around 40%–49% of the total precipitation (Houze 1977; Gamache and Houze 1983). The mesoscale anvil cloud is principally composed of ice crystals and contains a mesoscale updraft that creates only 25%–40% of its own condensate, the rest being supplied by the deep convective motions (Gamache and Houze 1983). Although we have some understanding of the causes of smaller-scale (2–20 km) convective motions, especially those producing isolated Cbs, the reasons for the existence of the mesoscale systems are not yet completely understood (cf. McAnelly and Cotton 1992). The question is, Why are isolated Cbs not a sufficient response of the atmosphere to the processes producing convective instability in the tropical atmosphere?

Our key finding is that, although exhibiting some variations between land and water and with time of day, these systems appear to form a single continuous size distribution with the number of clusters proportional to R^{-2}, when the observations are aggregated over monthly time periods and over large portions of the tropics. This observation implies a connection between objects that have been considered to be different, and requires some explanation. Satellite observations, alone, are unlikely to provide an explanation but we examine some of the main points of possible arguments to highlight the issues.

One explanation is that all sizes of convective systems result from nonlinear turbulent dynamics acting on the initial small-scale convective instability. The source of energy is the release of the convective available potential energy (CAPE), at first, by many smaller Cbs and later by the organized mesoscale systems that evolve from the Cbs. Since the mesoscale convective

systems are larger than the scale directly forced by convective instabilities, namely, the scale of individual Cb clouds, the cascade of energy from the supply at smaller scales to the dissipation at larger scales could produce an R^{-2} size spectrum if the atmosphere is able to attain a near equilibrium of energy transfer between different spatial scales. This behavior is consistent with the evolution of the cloud cluster spectrum during the diurnal cycle noted by Machado et al. (1993). In the early afternoon, there is a large increase of cloud cover by small clouds; the larger systems appear later near midnight by which time the equipartition of area covered by the whole range of cloud cluster sizes is accomplished.

Since the initial forcing of convection due to surface solar heating undergoes a strong diurnal modulation on land, where the majority of the larger CS appears, there may not be enough time for purely turbulent processes to create the mesoscale-sized systems. On the other hand, this could explain why the larger systems occur less frequently; namely, the larger systems may be produced only when enough small-scale convection occurs at the same time. Once the mesoscale systems are created, they seem able to sustain themselves over a few diurnal cycles (e.g., Miller and Fritsch 1991), possibly because of the radiative heating caused by the anvil clouds. However, the energy cascade explanation gives no clear role to the dynamical interactions and cloud radiative and microphysical processes observed to be occurring in and apparently modifying the organization of the mesoscale systems. Some studies have emphasized the importance of the synoptic "preconditioning" to the occurrence of these larger systems, although the large-scale motions do not appear to be strong enough to directly force the mesoscale motions (Cotton and Anthes 1989). Processes that limit the size of CS have not been identified, but finite size could be a consequence of a finite growth rate and continuing interaction with the large scale, which determine how long the conditions for growth last.

The logically opposite supposition is that the synoptic motions are necessary to produce the mesoscale convective systems. This may occur because the synoptic-scale motions are unable to exploit the available potential energy in a convectively unstable atmosphere, so that the first response by the atmosphere is the small-scale convection, but then this convection is organized into a more efficient mesoscale motion by the synoptic motions. In this case, synoptic-scale motions do not trigger convection but take advantage of it as a source of energy.

A third possibility is that the mesoscale systems result from the operation of some new dynamic instability that is triggered by the interaction of the convection and synoptic motions (e.g., Leary and Houze 1979; Raymond 1987; McAnelly and Cotton 1992). Our radiation calculations indicate that dynamically significant heating–cooling rates are produced by the clouds that appear to reinforce the warm-core vortex at the center of the mesocirculation (see Chen and Cotton 1988). Latent heating or cooling have also been proposed as causing mesocirculations (e.g., Zhang and Fritsch 1987; Zhang 1992). Thus, cloud radiative and/or latent energy feedbacks might become a new "slower" source of energy that plays some role in initiating the next growth phase.

The problem with both of the alternative explanations is that neither of them provides an explanation of why the size distribution of all CS forms a single continuum, which is our primary result. Further studies of the interaction and evolution of CS of all sizes require combining observations from satellite, surface, and in situ instruments with dynamical models that simulate full microphysics, radiation, and multiple convective plumes. One key observable is whether a mesoscale CS grows from one Cb, occasionally, or whether many Cbs combine to form the larger system. This question might be addressed with a satellite survey of CS that keeps track of the history of each CS through its lifetime. The data would need a spatial and temporal resolution of at least 1–2 km and 30 min to identify individual Cbs and smaller CS and to study their structural development.

b. CS structures

In section 3 we discuss the variability associated with the average cloud properties and note that the differences in average CS properties with size are relatively small compared to the variability within each size class. This fact may indicate that each size range contains a mixture of different stages in the life cycle of CS. Even if each CS size category represents a distinct life stage, we do not know how direct the relation between size and life stage really is. We note, however, that the CS with any Cb in the first size class (about 10%–20% of this size class) are composed predominantly of Cb clouds, whereas the remaining 80%–90% are composed solely of thinner anvil clouds. We might associate the first type of CS with the formative (Cb only) stage and the second type with fragments of the anvil in the dissipating stage. Moreover, Fig. 6 shows that the probability of CS to occur without convection (the dissipating stage) decreases as size increases, with about 15% of the larger CS over ocean lacking convective cells and less than 10% over land. This difference may be associated with the threshold used to define "convective pixels" but may also reflect a shorter lifetime for land CS as compared with ocean CS.

Given the aforementioned uncertainties, we identify formative stage CS with CS in the first size class (0–60 km) containing deep convection, dissipation stage CS as *any* sized CS having no "convective pixels" (albedo larger than 0.7), and mature stage CS as any larger ($R > 60$ km) CS that contain convective cells (Table 3). Future work should include a more advanced clas-

TABLE 3. Proportion of area covered by all convective cloud systems identified as being in the formative, mature, and dissipating stages of their life cycle. All values are in percent.

Surface type	Formative stage	Mature stage	Dissipating stage
Ocean	0.9	65.0	34.1
Land	1.3	73.4	25.3

sification based on others properties of the CS such as the shape of the whole CS, the arrangement of Cb within the CS, the area and partitioning of clouds among varying optical thickness and cloud-top height categories.

With a different definition of formative CS—for example, CS having more than 50% of their area covered by deep convection regardless of size—the area fraction covered by the formative stage increases by 2.3% (for 75% deep convection, the area increases by 0.15%). If a different definition of the mature stage CS is applied—for example, CS having more than 5% convective pixels—the area fraction of CS in the mature stage decreases by 9.7%. If an albedo threshold of 0.8 is used to define deep convection instead of 0.7, the mature CS area fraction decreases by 13.0%. Based on these definitions, about 1% of the CS cloud cover is in the formative stage and about 30% in the dissipating stage; the rest (about 70%) are mature systems (Table 3).

On average, mature CS are composed of 20% Cb and 80% MAC. The proportion of the convective part is a little higher (5%) when computed for the daily mean using an infrared threshold TC < 215 K to define deep convection. Houze (1982) and Johnson (1984) suggested a similar partitioning of the convective cloud area; Tao and Simpson (1989) found an 86.8% stratiform fraction in a model of squall lines. Despite some sensitivity of the fractions occupied by each cloud type to the thresholds used to separate them and the large variability of the cloud properties, our results show that mature stage CS, which represent the longest part of the CS life cycle (Houze 1982), have about the same relative fractions of convection, "transition" anvil cloud, and cirrus anvil cloud, regardless of size. For further discussion, we separate the MAC in mature CS into the TAC (28% of the total CS area) and the CAC (52% of the total area).

Houze (1977), Leary and Houze (1979), and Akaeda et al. (1991) illustrate the cloud cluster life cycle as viewed by radar and satellite. Their schematic life cycle shows that as the whole CS size grows the size of the deep convective part also increases from the formative to mature stages and then exhibits a faster decline from the mature to the dissipation stages. Zipser (1978) also concluded that once the deep convection develops strong mesoscale organization both the convection and the mesoscale circulation develop together. Zipser and LeMone (1980) found a positive correlation between convective vertical velocity and core diameter; Betts (1973) found a linear relation between the cumulus system size and cloud-top height. Convective clouds with higher tops also have larger rain rates than with lower ones (Leary 1984). Thus, a stronger updraft implies larger horizontal size and vertical extent of the convective system associated with more precipitation. Our results show some of the same relations: a positive correlation between convective cloud-top height and convective and anvil cloud area.

Houze (1982) proposed a conceptual structure for the evolution of these systems, where the convective motions feed water into the stratiform part and decay, while the stratiform part persists for a longer period. Leary (1984) found a lag of some hours between the convective precipitation and the development of the stratiform precipitation in the early stages of the life of mesoscale systems (cf. Fu et al. 1990). The stratiform anvil cloud appears to have an important function in the life cycle of the cloud cluster, since formation of this part reduces water transport by the updraft in the convective region. If this quantity of condensed water had to rain out in the convective towers, the downdrafts would probably quickly destroy the convection. Our results also show a positive correlation between convective cloud-top height (associated with convective updraft strength) and anvil cloud optical thickness (related to water content).

Leary and Houze (1979) and Houze (1982) describe the dissipating stage as having the following characteristics: a cessation of both active convection and stratiform precipitation, and slow dissolution of the stratiform cloud until only a few scattered fragments remain. We find high clouds without convection mostly in the smaller size ranges but about 10% of even the largest cloud systems lack convection.

We propose that the relationships diagnosed from these radar and aircraft studies (cf. Houze 1989) explain the correlations between the size and other properties of the CS that we observe, if we postulate that a CS will appear in different parts of the size distribution as it goes through its development and decay with changing fractions of convective and stratiform cloud parts. Thus, we have interpreted the structures of different-sized CS using the scheme shown in Fig. 5.

c. Cloud radiative effects

The CS cloud radiative effects, calculated with cloud properties that are constant all day, were relatively small at the top of the atmosphere; however, this nearly zero effect is misleading because it is composed of nearly canceling heating and cooling effects that occur at distinctly different levels in the tropical atmosphere. The general effects of surface cooling and atmospheric heating can decrease shallow convection and have an important cooling effect on the climate, for example. The cooling effect is larger over oceans than land be-

cause of the difference in surface albedo. The vertical profiles of the radiative heating and cooling suggest that the cloud radiative effects may be important to the mesoscale dynamics of these systems (cf. Chen and Cotton 1988), which in turn may affect the larger atmospheric circulation. The mesoscale anvil radiative effect acts to destabilize the middle atmosphere, reinforcing the mesoscale circulation, which in turn encourages more convection.

Our discussion of the radiative effects is somewhat uncertain because of uncertainties in water vapor and aerosol profiles and their spatial and temporal variability and in the accuracy of the ISCCP retrievals. Nevertheless, we believe that these calculations do suggest the importance of cloud-radiative effects on these systems. However, a more important source of uncertainty in determining the CS radiative effects is that we have neglected the systematic diurnal and size-related variations of the CS cloud properties. As a test of the importance of these variations, we computed the CS radiative effect supposing that the CS development stages occur at different hours of the day. In this calculation we used the proportional area covered and cloud properties of each development stage (Table 3), where the formative stage is equal to Cb; the mature stage is the average CS composed of Cb, TAC, and CAC; and the dissipative stage is CAC. The first test used the life cycle suggested by Miller and Fritsch (1991): formative stage in the afternoon, mature stage during the late afternoon to early morning, and dissipating stage in the morning. This cycle resembles the land diurnal variations. The resulting CS radiative effect at the top of the atmosphere for the ocean changes from -5.4 (no diurnal cloud variation) to -2.1 W m^{-2} and for the land from -3.0 to $+4.4$ W m^{-2}. Since the mature stage occurs during the night (principally a net heating effect), CS with this life cycle might heat the climate rather than cool it as usually supposed. Another simulation supposes the occurrence of the formative stage in early morning, the mature stage during the daytime, and the dissipating stage at night, similar to the ocean diurnal cycle. The results show an increase in the cooling effect for the ocean to -7.9 W m^{-2} and for the land to -6.3 W m^{-2}. We conclude that the determination of the actual net radiative effect of tropical CS requires not only more accurate determination of the cloud properties but also more attention to and better treatment of the variations of their properties with size and time of day and the phasing of their life cycle with respect to the diurnal cycle of solar irradiance and surface temperatures.

6. Summary

We summarize our main findings.

1) The most important features of the geographic distribution of tropical CS are that they occur more frequently over land than ocean and that there are not large differences in the geographic distribution of CS with size. The first feature also means that as the locus of vigorous convection shifts hemisphere with the seasons there is a seasonal hemispheric asymmetry of the amount of CS associated with the different ratios of land and ocean area in the two hemispheres. The highest concentration of CS occurs over South America, while the largest area covered by CS is in the western Pacific. These basic features can also be identified in the combined results of Velasco and Fritsch (1987) and Miller and Fritsch (1991).

2) The shape of the CS size distribution is similar over the whole tropics except for a small systematic land–ocean difference. Explanation of the formation of the larger (scale greater than 200 km) convective systems from the initial small-scale (<20 km) convective disturbances must account for this size distribution. The small enhancement of the frequency of larger CS during the one El Niño we examined is similar in magnitude to the interannual variability. On land, the smallest CS occur somewhat more frequently and the largest CS occur somewhat less frequently than over oceans. These size distribution differences, together with larger diurnal variations of convection over land, suggest that the evolution time scales for land CS may be shorter than over ocean.

3) The average cloud properties of CS suggest a division into a part (about 20%) representing active convection and a part (about 80%) representing the mesoscale stratiform anvil clouds. The convective clouds have cloud-top pressures about 50 mb lower and optical thicknesses about six times larger than the mesoscale anvil clouds. Since the vertical extent of the convective cloud is only about twice that of the anvil cloud, the water content of the convective cloud must be about three times larger than that of the anvil cloud. About one-third of the anvil cloud area is composed of clouds that are about three to four times optically thicker than the remainder of the anvil clouds; these thicker clouds may be associated with the (stratiform) precipitating portion of the mesoscale anvil clouds. The fraction of the cloud area occupied by convective clouds is nearly constant over all sizes of CS. The convective cloud-top pressure decreases with increasing system size, while the anvil optical thickness increases with increasing system size. The convective cloud optical thickness and the anvil cloud-top pressure vary little with system size. All of the cloud property variations with convective system size are correlated, consistent with other observations of correlations between convective updraft strength and CS vertical extent and horizontal size.

4) The variations of average cloud properties, structure, Cb fraction, and probability of Cb occurrence with the size of the CS suggest a classification into "life stages." The larger CS, where the fraction of Cb is nearly constant, appear to be similar in character to the "maximum extent" stage identified by others as the mature CS stage. The smaller CS appear to comprise

systems containing convection with little anvil cloud or systems with anvil cloud but no convection. These two types can be identified as the formative and dissipating stages, respectively. Some larger CS without Cb also occur. This interpretation, together with the correlations of updraft and CS extent observed by others and the correlations of cloud properties with CS size that we have found suggest that the magnitude of the convective updraft and mass (and water) flux at the base of the Cb may determine the average vertical and horizontal extent and mean cloud properties of all CS.

5) The local radiative effect (daily mean) of the CS clouds is generally a positive change in atmospheric net fluxes (decrease in cooling), which reinforces the latent heating of the system. The profile of the radiative heating and cooling shows that radiation destabilizes the whole anvil cloud layer, destabilizes the convection near its top, and stabilizes the convection near its base at the planetary boundary layer top. The magnitudes of the radiative heating–cooling rates are large enough that they may play a significant role in the dynamical development of the mesoscale CS. In particular, over land, the destabilization of the anvil cloud may help sustain CS during the nighttime when their convective source of energy is reduced, whereas the stabilization of the PBL top may amplify the diurnal cycle of convection. Most analyses of the energy and water budgets of these systems have used approximate daily mean or composited life stage observations; more attention to the diurnal and size variations of the convective and radiative contributions is needed to understand the development of these systems.

6) The radiative effects of the mesoscale anvil cloud dominate the total effect of CS; hence, their properties and changes, which may be under the direct control of the convection, are more important to determining the radiative effect of tropical cloudiness on climate. If we hold the average CS cloud properties constant over the diurnal cycle, their overall radiative effect is nearly zero (slight cooling) at the top of the atmosphere, a somewhat larger cooling at the surface, and a net heating of the atmosphere. However, the actual radiative effect is dependent on the diurnal variation of the CS cloud properties and the correlation of the life cycle of CS with the diurnal cycle because of systematic variations of cloud properties with system size. Moreover, the small changes in net flux depend on the surface and atmospheric properties as well. All of these factors make determination of radiative feedbacks very difficult, since even a change of geographic location or diurnal phase without a change of mean cloud properties could produce a significant feedback. Moreover, it is only the area-averaged effects that are so small; the local radiative effects produce heating–cooling gradients that may influence atmospheric motions. The important point of all these conclusions is that the climatic importance of the radiative effects of convective clouds may be realized more through their effect on tropical (and global) atmospheric dynamics than through their direct effect on the planetary radiation balance.

This work represents an early attempt to survey the physical properties and structure of the clouds in tropical convective systems from satellite observations; many of our findings only suggest the interpretations we have presented. We need to extend this analysis to more data to improve statistical significance, to include classifications based on the internal structure of the CS, to track individual systems to determine their evolution, and to combine satellite measurements with other atmospheric measurements (particularly surface radar and passive microwave measurements) for a more complete diagnosis. Two key opportunities for this type of analysis, extending the technique of Tollerud and Esbensen (1985), are presented by the Tropical Ocean–Global Atmosphere Coupled Ocean–Atmosphere Response Experiment (TOGA COARE) and the planned GEWEX (Global Energy and Water Cycle Experiment) Continental-Scale International Project.

Acknowledgments. The organization of this paper benefited from thoughtful comments of two anonymous reviewers. We also benefitted from conversations with A. Del Genio and M. Fritsch. We thank A. Walker for assistance with data processing. One of us (L.A.T.M.) acknowledges support from the Columbia University Global Change Institute (R. Levenson) to visit NASA Goddard Institute for Space Studies. This research is supported by the NASA Climate Program (J. Dodge). The ISCCP project manager is R. Schiffer.

REFERENCES

Akaeda, K., T. Yokoyama, A. Tabata, M. Ishihara, and H. Sakakibara, 1991: Evolution of the kinematic structure within a mesoscale convective system in the growing and mature stages. *Mon. Wea. Rev.*, **119**, 2664–2676.

Arkin, P. A., and P. E. Ardanuy, 1989: Estimating climatic-scale precipitation from space: A review. *J. Climate*, **2**, 1229–1238.

Betts, A. K., 1973: A relationship between stratification, cloud depth and permitted cloud radii. *J. Appl. Meteor.*, **12**, 890–893.

Byers, H. R., and R. R. Braham, 1949: *The Thunderstorms.* U.S. Government Printing Office, 287 pp.

Chen, S., and W. R. Cotton, 1988: The sensitivity of a simulated extratropical mesoscale convective system to longwave radiation and ice-phase microphysics. *J. Atmos. Sci.*, **45**, 3897–3910.

Churchill, D. D., and R. A. Houze, 1984: Development and structure of winter monsoon cloud clusters on 10 December 1978. *J. Atmos. Sci.*, **41**, 933–960.

Cotton, W. R., and R. A. Anthes, 1989: *Storm and Cloud Dynamics.* Academic Press–Harcourt Brace Jovanovich, 880 pp.

——, M.-S. Lin, R. L. McAnelly, and C. J. Tremback, 1989: A composite model of mesoscale convective complexes. *Mon. Wea. Rev.*, **117**, 765–783.

Cox, S. K., D. S. McDougal, D. A. Randall, and R. A. Schiffer, 1987: FIRE—The First ISCCP Regional Experiment. *Bull. Amer. Meteor. Soc.*, **68**, 114–118.

Desbois, M., T. Kayiranga, B. Gnamien, S. Guessous, and L. Picon, 1988: Characterization of some elements of the Sahelian climate and their inter-annual variations for July 83, 84 and 85 from

the analysis of METEOSAT ISCCP data. *J. Climate,* **1,** 867–904.

Duvel, J. P., 1989: Convection over tropical Africa and Atlantic Ocean during northern summer. Part I: Interannual and diurnal variations. *Mon. Wea. Rev.,* **117,** 2782–2799.

——, 1990: Convection over tropical Africa and Atlantic Ocean during northern summer. Part II: Modulation by easterly waves. *Mon. Wea. Rev.,* **118,** 1855–1868.

Ellingson, R. G., and Y. Fouquart, 1991: The intercomparison of radition codes used in climate models: Longwave results. *J. Geophys. Res.,* **96,** 8925–8953.

Esbensen, S. K., J. T. Wang, and E. Tollerud, 1988: A composite life cycle of nonsquall mesoscale convective systems over the tropical ocean. Part II: Heat and moisture budgets. *J. Atmos. Sci.,* **45,** 538–548.

Fels, S. B., J. T. Kiehl, A. A. Lacis, and M. D. Schwarzkopf, 1991: Infrared cooling rate calculations in operational general circulation models: Comparisons with benchmark computations. *J. Geophys. Res.,* **96,** 9105–9120.

Fouquart, Y., B. Bonnel, and V. Ramaswamy, 1991: Intercomparing shortwave radiation codes for climate studies. *J. Geophys. Res.,* **96,** 8955–8968.

Frank, W. M., 1978: The life cycles of GATE convective systems. *J. Atmos. Sci.,* **35,** 1256–1264.

Fu, R., A. D. Del Genio, and W. B. Rossow, 1990: Behavior of deep convective clouds in the tropical Pacific deduced from ISCCP radiances. *J. Climate,* **3,** 1129–1152.

Gamache, J. F., and R. A. Houze, 1982: Mesoscale air motions associated with a tropical squall line. *Mon. Wea. Rev.,* **110,** 118–135.

——, and ——, 1983: Water budget of a mesoscale convective system in the tropics. *J. Atmos. Sci.,* **40,** 1835–1850.

Gray, W. M., and R. W. Jacobson, 1977: Diurnal variation of deep cumulus convection. *Mon. Wea. Rev.,* **105,** 1171–1188.

Hansen, J., G. Russell, D. Rind, P. Stone, A. Lacis, S. Lebedeff, R. Ruedy, and L. Travis, 1983: Efficient three-dimensional global models for climate studies: Models I and II. *Mon. Wea. Rev.,* **111,** 609–662.

Hobbs, P. V., 1978: Organization and structure of clouds and precipitation on the mesoscale and microscale in cyclonic storms. *Rev. Geophys. Space Phys.,* **16,** 741–755.

Holland, G. J., J. L. McBride, R. K. Smith, D. Jaspar, and T. D. Keemon, 1986: The BMRC Australian Monsoon Experiment: AMEX. *Bull. Amer. Meteor. Soc.,* **67,** 1466–1472.

Houze, R. A., 1977: Structure and dynamics of a tropical squall-line system. *Mon. Wea. Rev.,* **105,** 1540–1567.

——, 1982: Cloud clusters and large-scale vertical motions in the tropics. *J. Meteor. Soc. Japan,* **60,** 396–409.

——, 1989: Observed structure of mesoscale convective systems and implications for large-scale heating. *Quart. J. Roy. Meteor. Soc.,* **115,** 425–461.

——, and A. K. Betts, 1981: Convection in GATE. *Rev. Geophys. Space Phys.,* **19,** 541–576.

——, and P. V. Hobbs, 1982: Organization and structure of precipitating cloud systems. Vol. 41, *Advances in Geophysics,* Academic Press, 3405–3411.

Janowiak, J. E., and P. A. Arkin, 1991: Rainfall variations in the tropics during 1986–1989, as estimated from observations of cloud-top temperature. *J. Geophys. Res.,* **96,** 3359–3373.

Johnson, R. H., 1984: Partitioning tropical heat and moisture budgets into cumulus and mesoscale components: Implications for cumulus parameterization. *Mon. Wea. Rev.,* **112,** 1590–1601.

——, and G. S. Young, 1983: Heat and moisture budgets of tropical mesoscale anvil clouds. *J. Atmos. Sci.,* **40,** 2138–2147.

——, and R. A. Houze, 1987: Precipitation cloud systems of the Asian monsoon. *Monsoon Meteorology,* C.-P. Chang and T. N. Krishnamurti, Eds., Oxford University Press, 298–353.

——, and J. F. Bresch, 1991: Diagnosed characteristics of precipitation systems over Taiwan during the May–June 1987 TAMEX. *Mon. Wea. Rev.*. **119,** 2540–2557.

Jorgensen, D. P., and M. A. LeMone, 1989: Vertical velocity characteristics of oceanic convection. *J. Atmos. Sci.,* **46,** 621–640.

——, E. J. Zipser, and M. A. LeMone, 1985: Vertical motions in intense hurricanes. *J. Atmos. Sci.,* **42,** 839–856.

Lacis, A. A., and V. Oinas, 1991: A description of the correlated k distribution method for modeling nongray gaseous absorption, thermal emission, and multiple scattering in vertically inhomogeneous atmospheres. *J. Geophys. Res.,* **96,** 9027–9063.

Leary, C. A., 1984: Precipitation structure of the cloud clusters in a tropical easterly wave. *Mon. Wea. Rev.,* **112,** 313–325.

——, and R. A. Houze, 1979: The structure and evolution of convection in a tropical cloud cluster. *J. Atmos. Sci.,* **36,** 437–457.

——, and E. N. Rappaport, 1987: The life cycle and internal structure of a mesoscale convective complex. *Mon. Wea. Rev.,* **115,** 1503–1527.

Machado, L. A. T., M. Desbois, and J.-P. Duvel, 1992: Structural characteristics of deep convective systems over tropical Africa and Atlantic Ocean. *Mon. Wea. Rev.,* **120,** 392–406.

——, J.-P. Duvel, and M. Desbois, 1993: Diurnal variations and modulation by easterly waves of the size distribution of convective cloud clusters over West Africa and the Atlantic Ocean. *Mon. Wea. Rev.,* **121,** 37–49.

McAnelly, R. L., and W. R. Cotton, 1992: Early growth of mesoscale convective complexes: A meso-β-scale cycle of convective precipitation? *Mon. Wea. Rev.,* **120,** 1851–1877.

Maddox, R. A., 1980: Mesoscale convective complexes. *Bull. Amer. Meteor. Soc.,* **61,** 1374–1387.

——, 1983: Large-scale meteorological conditions associated with midlatitude, mesoscale convective complexes. *Mon. Wea. Rev.,* **111,** 1475–1493.

——, D. J. Perkey, and J. M. Fritsch, 1981: Evolution of upper tropospheric features during the development of a mesoscale convective complex. *J. Atmos. Sci.,* **38,** 1664–1674.

Miller, D., and J. M. Fritsch, 1991: Mesoscale convective complexes in the western Pacific region. *Mon. Wea. Rev.,* **119,** 2978–2992.

Minnis, P., and E. F. Harrison, 1984: Diurnal variability of regional cloud and clear sky radiative parameters derived from GOES data. Part III: November 1978 radiative parameters. *J. Climate Appl. Meteor.,* **23,** 1032–1051.

——, P. W. Heck, and D. F. Young, 1993: Inference of cirrus cloud properties from satellite-observed visible and infrared radiances. Part II: Verification of theoretical cirrus radiative properties. *J. Atmos. Sci.,* **50,** 1305–1322.

Nakasawa, T., 1988: Tropical super clusters within intraseasonal variations over the western Pacific. *J. Meteor. Soc. Japan,* **66,** 823–839.

NOAA, 1976: *U.S. Standard Atmosphere, 1976,* Publication NOAA-S/T76-1562. U.S. Government Printing Office.

Parsons, D. B., and P. V. Hobbs, 1983: The mesoscale and microscale structure and organization of clouds and precipitation in midlatitude cyclones. VII: Formation, development, interaction and dissipation of rainbands. *J. Atmos. Sci.,* **40,** 559–579.

Payne, S. W., and M. M. McGarry, 1977: The relationship of satellite inferred convective activity to easterly waves over west Africa and the adjacent ocean during Phase III of GATE. *Mon. Wea. Rev.,* **105,** 413–420.

Raymond, D. J., 1987: A forced gravity-wave model of self-organizing convection. *J. Atmos. Sci.,* **44,** 3528–3543.

Rossow, W. B., and R. A. Schiffer, 1991: ISCCP cloud data products. *Bull. Amer. Meteor. Soc.,* **72,** 2–20.

——, and L. C. Garder, 1994a: Cloud detection using satellite measurements of infrared and visible radiances for ISCCP. *J. Climate,* **7,** in press.

——, and ——, 1994b: Validation of ISCCP cloud detection. *J. Climate,* **7,** in press.

——, ——, and A. A. Lacis, 1989: Global, seasonal cloud variations from satellite radiance measurements. Part I: Sensitivity of analysis. *J. Climate,* **2,** 419–458.

——, ——, P.-J. Lu, and A. Walker, 1991: International Satellite Cloud Climatology Project (ISCCP) documentation of cloud

data. WMO/TD No. 266, World Climate Research Programme (ICSU/WMO), 75 pp. + 3 appendixes.

Schiffer, R. A., and W. B. Rossow, 1983: The International Satellite Cloud Climatology Project (ISCCP): The first project of the World Climate Research Program. *Bull. Amer. Meteor. Soc.*, **64,** 779–784.

Schiffer, R. A., and W. B. Rossow, 1985: ISCCP global radiance data set: A new resource for climate research. *Bull. Amer. Meteor. Soc.*, **66,** 1498–1505.

Scorer, R., 1977: *Clouds of the World.* Lothian, 176 pp.

Sohn, B.-J., and E. A. Smith, 1992: Global energy transports and the influence of clouds on transport requirements—A satellite analysis. *J. Climate,* **5,** 717–734.

Stephens, G. L., and T. S. Greenwald, 1991: The earth's radiation budget and its relation to atmospheric hydrology, 2, Observation of cloud effects. *J. Geophys. Res.*, **96,** 15 325–15 340.

——, G. W. Paltridge, and C. M. R. Platt, 1978: Radiation profiles in extended water clouds. III: Observations. *J. Atmos. Sci.*, **35,** 2133–2141.

Takahashi, T., 1990: Near absence of lightning in torrential rainfall producing Micronesian thunderstorms. *Geophys. Res. Lett.*, **17,** 2381–2384.

Tao, W.-K., and J. Simpson, 1989: Modeling study of a tropical squall-type convective line. *J. Atmos. Sci.*, **46,** 177–201.

Tollerud, E. I., and S. K. Esbensen, 1985: A composite life cycle of nonsquall mesoscale convective systems over the tropical ocean. Part I: Kinematic fields. *J. Atmos. Sci.*, **42,** 823–837.

Trenberth, K. E., and G. W. Branstator, 1992: Issues in establishing causes of the 1988 drought over North America. *J. Climate,* **5,** 159–172.

Velasco, I., and J. M. Fritsch, 1987: Mesoscale convective complexes in the Americas. *J. Geophys. Res.*, **92,** 9591–9613.

Warren, S. G., C. J. Hahn, J. London, R. M. Chervin, and R. L. Jenne, 1986: Global distribution of total cloud and cloud type amounts over land. NCAR Tech. Note TN-273, 29 pp. + 200 maps. [NTIS DE87-00-6903.]

——, ——, ——, ——, and ——, 1988: Global distribution of total cloud and cloud type amounts over the ocean. NCAR Tech. Note TN-317, 42 pp. + 170 maps. [NTIS DE90-00-3187.]

Webster, P. J., and G. L. Stephens, 1980: Tropical upper-tropospheric extended clouds: Inferences from Winter MONEX. *J. Atmos. Sci.*, **37,** 1521–1541.

——, and R. A. Houze, 1991: The Equatorial Mesoscale Experiment (EMEX): An overview. *Bull. Amer. Meteor. Soc.*, **72,** 1481–1505.

Weisman, M. L., 1992: The role of convectively generated rear-inflow jets in the evolution of long-lived mesoconvective systems. *J. Atmos. Sci.*, **49,** 1826–1847.

Wielicki, B. A., and R. M. Welch, 1986: Cumulus cloud properties derived using LANDSAT satellite data. *J. Climate Appl. Meteor.*, **25,** 261–305.

Zhang, D.-L., 1992: The formation of a cooling-induced mesovortex in the trailing stratiform region of a midlatitude squall line. *Mon. Wea. Rev.*, **120,** 2763–2785.

——, and J. M. Fritsch, 1987: Numerical simulation of the meso-β scale structure and evolution of the 1977 Johnstown flood. Part II: Inertially stable warm-core vortex and the mesoscale convective complex. *J. Atmos. Sci.*, **44,** 2593–2612.

Zipser, E. J., and C. Gautier, 1978: Mesoscale events within a GATE tropical depression. *Mon. Wea. Rev.*, **106,** 789–805.

——, and M. A. LeMone, 1980: Cumulonimbus vertical velocity events in GATE. Part II: Synthesis and model core structure. *J. Atmos. Sci.*, **37,** 2458–2469.